# p53 restores the silencing of activated L1 Transposons

Pratyashaa Paul[1], Arun Kumar[1], Astik Kumar De[1], Ankita Subhadarsani Parida,[1] Satyajeet Khatua[1], Gauri Bhadke[1], Fizalin Pattanayak[1], Bhavana Tiwari[1#]

[1]Department of Biological Sciences, Indian Institute of Science Education and Research Berhampur, India

[#]Correspondence: btiwari@iiserbpr.ac.in

Department of Biological Sciences,
Indian Institute of Science Education and Research Berhampur,
Berhampur, Odisha 760010, India

**Abstract**

LINE1/L1 transposons, comprising around 20% of the human genome, typically remain quiescent in healthy somatic cells but become activated in various cancer types. Our recent investigation reveals that p53 acts on L1 promoter to supress these repetitive sequences, potentially constituting a tumor suppressive pathway. In this study, we observe that p53 silences L1mRNA-cDNA hybrids (trans R-loops) formed during retrotransposition. We show that activation of L1 by HDAC inhibitors (HDACi) leads to the accumulation of L1mRNA-cDNA hybrids in p53$^{-/-}$ cells, which were mitigated by treatment with the reverse transcriptase inhibitor. Furthermore, we demonstrate that p53 aids in re-silencing of hyperactivated L1 induced by HDACi by recruiting histone repressive marks, specifically H3K9me3 and H3K27me3 to the L1-5'UTR and inhibiting the deposition of H3K4me3 and H3K9ac marks. This study highlights a novel role of p53 in reinstating the suppression of activated L1 and regulating R-loops derived from retrotransposition, thus maintaining genome stability and modulating the expression of inflammatory genes.

**In Brief:** The role of L1 transposon derived L1mRNA-cDNA hybrids in DNA damage and inflammation is not clear. Paul et al. reveals that p53 prevents L1cDNA derived RNA-DNA hybrids to control DNA damage and activation of inflammatory genes. The findings also elucidate the role of p53 in initiating the repression of activated transposons by facilitating the recruitment of epigenetic repressive marks and preventing the deposition of activating marks at L1-5'UTR.

"**Keywords:** p53, L1/LINE-1, R-loops, RNA-DNA hybrids, Cis R-loop, Trans R-loop, Transposons, HDAC inhibitors

**Highlights**

1. p53 loss facilitates accumulation of both cis (L1mRNA-gDNA) and trans (L1mRNA-cDNA) forms of L1 R-loops derived RNA-DNA hybrids.
2. The youngest, actively retrotransposing full-length L1s contribute to the formation of trans (L1mRNA-cDNA) R-loops.
3. p53 aids immediate L1 re-silencing by restoring deposition of epigenetic repressive and inhibition of activating marks.
4. Reverse transcriptase inhibitor prevents L1 mediated DNA damage.

**Subject Categories**: L1/LINE-1, p53, Retrotransposons, RNA-DNA hybrids, Cis R loops, Trans R-loop, L1/LINE-1

48

49 **Introduction**

50 p53 is the most commonly mutated tumour suppressor gene [1] and activates its downstream effectors
51 to regulate cell cycle, apoptosis and senescence pathways to maintain genome integrity [2]. Recent
52 studies have shown that p53 represses mobile genetic elements, suggesting a new axis of tumor
53 suppression [3-6]. p53 mediated retroelement repression is conserved across various species,
54 including flies, fish, and human somatic cell lines [7-10]. Employing CRISPR-mediated wild-type (wt)
55 and p53 knockout ($p53^{-/-}$) cells, we have identified p53 binding motifs within the 5'UTR of L1
56 retrotransposons, and work from others predicted in Alu sequences [11-13]. By utilizing the synthetic
57 L1-5'UTR-egfp reporter system, we demonstrated that p53 maintains transrepression of L1 within
58 human somatic cell lines by facilitating the deposition of epigenetic repressive marks at the 5'UTR
59 promoter to exert its repressive function [9]. Several other studies have underscored a direct
60 correlation between increased retroelement expression and p53 mutations within cancer contexts
61 [5,14,15]. These collective observations prompted an exploration into the potential involvement of p53
62 in initiating the silencing of activated L1 transposons and delineating the underlying mechanisms of
63 *de novo* silencing. To address this, we employed HDAC inhibitors Trichostatin (TSA) and Sodium
64 Butyrate (NaB) drugs that are known to induce repetitive elements, including L1 transposons on wt
65 and $p53^{-/-}$ cells [16-18]. We examined the role of p53 in L1 resilencing function, a process that mirrors
66 the epigenetic reprogramming observed in early embryos and primordial germ cells *in vivo*.

67 The initiation of L1 retrotransposition process involves transcription followed by the
68 translation of two essential L1-encoded open reading frame proteins (ORFps); ORF1p and ORF2p.
69 The combined efforts of ORF1p and ORF2p facilitate L1 retrotransposition and are linked to various
70 diseases [19-23]. These proteins are crucial for the reverse transcription of L1cDNA and its subsequent
71 integration. During mobilization, these ORFs are transcribed by RNA pol II, leading to the formation
72 of a L1mRNA-gDNA hybrid as a transcriptional intermediate, if these structures persists can lead to
73 the formation of 'cis R-loops'. R-loops represent three-stranded nucleic acid structures composed of
74 an RNA/DNA hybrid alongside a displaced single-stranded DNA (ssDNA) and these can lead to
75 either physiological or pathological outcomes. L1 encoded ORF2 protein contains two functional
76 domains essential for target-primed reverse transcription: the Endonuclease (EN) domain creates a
77 single-stranded DNA nick for integration, and the Reverse Transcriptase (RT) domain primes
78 complementary DNA synthesis based on the L1mRNA template. The recent structural findings on
79 ORF2p identified domains that shows extensive interactions with RNA templates [24]. The reverse
80 transcription function of ORF2p generates a L1mRNA-cDNA hybrid structure, hence referred to as
81 'trans R-loop' intermediate structure comprising a free and un-nicked DNA segment, a nicked DNA,

82 the newly synthesized cDNA, and the L1mRNA serving as the template for reverse transcription,
83 probably the four stranded non-canonical form of R-loops. L1 derived cDNA acts as triggers for type
84 1 interferon response, leading to the formation of inflammasomes [25]. Ectopic accumulation of (cis) R
85 loops, particularly those arising from transcriptional events, is associated with various genomic and
86 epigenetic instabilities [26-28]. These R-loops are implicated in genome instability [29] and DNA damage
87 through several mechanisms: initiating abnormal replication [30], inducing transcription stress, and
88 facilitating collisions between transcription and replication processes [26]. Consequently, the
89 accumulation of cis and trans R-loops derived from L1 sequences can potentially lead to DNA
90 damage and inflammation, an aspect of L1 pathogenesis that remains unexplored. L1-derived
91 RNA/DNA hybrids may be exported to the cytosol via an as yet unidentified process, where they are
92 detected by sensors such as endosomal TLR3 and the membrane-bound cGAS inflammatory
93 pathway [31]. The L1 retroelement has the capability to retrotranspose Alus [32,33] and SVAs [34,35] hence
94 these elements can also participate in the generation of unscheduled R-loops in the genome. There
95 have been reports of ~100 L1-mediated insertions, the end product of retrotransposition, leading to
96 genetic diseases. These retroelement insertions have been linked to the transmission of congenital
97 disorders through the germ line, familial predispositions to cancer, as well as other conditions like β-
98 thalassemias, and hemophilias [36-38]. However, there is an increasing acknowledgment that active
99 L1s in somatic tissues also present inherent oncogenic hazard [3,5,15].
100 Herein, we establish the role of p53 in controlling the intermediate components of L1,
101 retrotransposition specifically L1mRNA-cDNA hybrids, referred to here as 'trans R-loops', formed
102 during reverse transcription, and its role in genome instability. We present evidence indicating that
103 the most recently evolved full-length retrotransposition-competent L1 elements are actively involved
104 in the generation of trans R-loops. This assertion is supported by our analysis of DRIP-seq (DNA-
105 RNA immunoprecipitation sequencing) data, along with validation conducted through DRIP-qCR
106 (quantitative PCR) experiments. Furthermore, our findings reveal that the over-expression of the RT
107 domain of L1-ORF2p led to a notable increase in trans R-loop accumulation, which was
108 accompanied by heightened levels of DNA damage and inflammation. Interestingly, treatment with
109 a reverse transcriptase inhibitor attenuated these elevations in DNA damage and inflammation
110 markers, underscoring the oncogenic implications of L1-derived trans R-loops. We also demonstrate
111 that p53 mediates *de novo* silencing of hyperactivated L1 retroelements employing HDAC inhibitor
112 (HDACi) treated cancer cell lines. Using synthetic L1-5'UTR-eegfp wt and p53$^{-/-}$ reporter cells,
113 combining with HDACi exposure, we observed highly derepressed L1 transposons in both the
114 genotypes. However, upon the withdrawal of HDACi drugs, the silencing of dereprssed L1
115 transposons and its retrotransposition intermediates was immediate in wt p53 cells but not in p53$^{-/-}$

116 cells. This restoration of L1 silencing in wt L1 reporter coincided with the recruitment of histone
117 repressive marks and the removal of activating marks at the L1-5'UTR providing insights into
118 potential therapeutic strategies for diseases associated with L1 activation.
119
120 **Results**
121 **p53 controls L1 retrotransposition intermediary components**
122 Recently, our research demonstrated that p53 plays a crucial role in suppressing L1 transposons at
123 the transcription levels in human cell lines under non-stress conditions [9]. Building upon these
124 findings, our current study delves into the consequences of p53 deficiency on the regulation of
125 intermediary by-products of L1 activity, specifically RNA-DNA hybrids formed during
126 retrotransposition. Here, we noted heightened levels of L1 transcripts (**Figures** 1A and B) and ORF1
127 protein (**Figures** 1C and 1D) in both cancer-derived p53$^{-/-}$ cell lines (A375 and U2OS) generated
128 using CRISPR cas9 methodology **(Figures** S1A and B**)**, consistent with our prior study [4]. The
129 immunofluorescence (IF) experiments in wt and p53$^{-/-}$ cells with s9.6, a widely used antibody to
130 visualize and detect the RNA-DNA hybrids of R-loops [39], showed an increased signal of cytoplasmic
131 RNA-DNA hybrids in p53$^{-/-}$ (**Figures** 1E and 1E') as compared to the parental wt cells. Next, DNA-
132 RNA immunoprecipitation (DRIP) assays were conducted utilizing the s9.6 antibody to investigate
133 the propensity of L1 element in the participation of R-loops in p53$^{-/-}$ cells (**Figure** 1F). In this
134 experiment s9.6 antibody was used to precipitate RNA-DNA hybrids structures followed by
135 quantification by qPCR using the primers that binds the DNA region of interest to measure the
136 binding [40]. Mapping experiments with DRIP-qPCR using primers spanning 5'UTR, ORF1, and ORF2
137 regions revealed that the L1-5'UTR region, which harbors RNA pol II promoter, was predominantly
138 enriched in R-loops derived RNA-DNA hybrids, whereas the ORF2 region exhibited a modest
139 enrichment. The specificity of our assay for detecting RNA-DNA hybrids was validated by pre-
140 treating the samples with RNase H before the antibody pulldown (data not shown), resulting in the
141 complete abolition of our ability to amplify the region. Given that the majority of the nuclear R-loop
142 derived RNA-DNA hybrids was observed in the cytoplasm, we leveraged an alternative method to
143 specifically probe R-loops. This involved the overexpression of RNaseH1 with D210N catalytic dead
144 mutant (RNH-GFP) with the nuclear localization signal fused at the N-terminus in A375 wt and p53$^{-}$
145 $^{/-}$ cells [27,40,41]. Similar GFP expression was observed between these genotypes. qPCR experiments
146 from GFP immunoprecipitated samples indicated stronger R-loop signal at L1-5'UTR and a weaker
147 signal at the gene body L1-ORF2 similar to s9.6 pull down data **(Figures** 1G and 1H**)**. Moreover, our
148 analysis of DRIP-seq and Global Run-On sequencing (GRO-seq) data unveils a partial overlap of
149 peaks between RNA-DNA hybrid sequences and nascent transcripts at the L1-5'UTR coordinates

150 (cis R-loops). Conversely, no overlapping peaks were observed at the L1-ORF2 region (**Figure** 1I),
151 suggesting that the 5'UTR region demonstrates a higher tendency to form cis R-loops, likely due to
152 nascent RNA annealing. Conversely, the ORF2 region may be involved in the generation of trans R-
153 loops, originating from distant L1mRNAs.
154
155 **p53 prevents the formation of L1 trans R-loop derived RNA-DNA hybrids**
156 During the retrotransposition life cycle, the full-length L1 undergoes a process in which it generates
157 an identical DNA copy of itself, known as L1cDNA, through the reverse transcription of L1mRNA.
158 Hence, within the retrotransposition life cycle, there is potential for the formation of two types of RNA-
159 DNA hybrids that can serve as R-loop; cis R-loops (L1mRNA-gDNA) occurring at the L1 5'-UTR
160 promoter level during transcription, and trans R-loops (L1mRNA-cDNA) formed during reverse
161 transcription. Genome-wide DRIP-seq studies reveal that cis R-loops are predominantly found in
162 GC-rich regions and promoters [42,43]. The recent findings demonstrate that p53 play a role in global
163 regulation of. cis R-loops and human papillomaviruses proteins induce R-loops in p53 inhibited cells
164 [44,45]. However, the prcise mechanism by which p53 regulates L1 derived R-loops has yet to be
165 explored. The analyses of DRIPseq data from IMR-90, HEK293T, and k562 cell lines harbouring p53
166 mutations (PMID: 26579211) revealed that young L1 subfamilies, which are capable of
167 retrotransposition, participate in R-loop formation **(Figure** 2A**)**. Further, to investigate whether L1
168 hyperactivation leads to increased accumulation of R loop formation, we treated A375 wt and p53$^{-/-}$
169 cells with an HDAC inhibitor **(Figure** 2B**)** Sodium Butyrate (NaB) **(Figure** 2C**).** RNAseq analyses on
170 NaB (PMID: 38410440, 38410440) and TSA (PMID: 37496675) exposed cells and qRT-PCR on NaB
171 treated A375 wt and p53$^{-/-}$ did, in fact, show that L1 expression was elevated upon HDAC inhibition
172 (**Figures** 2C and 2D). IF assays on wt and p53$^{-/-}$ cells treated with NaB revealed an increased signal
173 of s9.6 detecting the RNA-DNA hybrids **(Figures** 2E and 2E'**)**. Significantly, rescue experiments
174 employing 3TC, a well-known reverse transcriptase inhibitor inhibiting L1cDNA formation, led to
175 decreased s9.6 signals in both NaB-treated wild-type (wt) and p53$^{-/-}$ cells. This implicates the L1
176 reverse transcription process in generating L1 R-loops (L1mRNA-cDNA) derived RNA-DNA hybrids
177 (**Figures** 2E and E'). Subsequent qRT-PCR analysis of RNA-DNA hybrids isolated by s9.6
178 immunoprecipitation from A375 wt and p53$^{-/-}$cells, upon 3TC treatment, demonstrated complete
179 depletion of R-loops from the L1-ORF2 region, with a modest reduction observed at the 5'-UTR
180 (**Figure** 2F). This verifies the likelihood of L1-ORF2 being prone to trans R-loop formation. Similar
181 outcomes were obtained via immunoprecipitation using a GFP antibody from cells expressing RNH-
182 GFP (**Figure** 2G). These findings underscore that although the majority of the L1 5'-UTR region
183 contributes to cis R-loop formation, L1-ORF2 likely facilitates trans R-loop formation, highlighting the

184 involvement of L1 in both types of R-loop signals, arising from L1mRNA-gDNA as well as L1mRNA-
185 cDNA hybrids.
186 Next, we conducted overexpression of L1-encoded proteins- ORF1p, EN and RT enzymatic
187 domains of ORF2p c-terminally fused with GFP and empty vector (EV) as a negative control, in $p53^{-}$
188 $^{/-}$ cells of A375 and U2OS cell to investigate the potential impact of these overexpressed proteins on
189 the abundance of RNA-DNA hybrids. It has been established that the RT domain maintains reverse
190 transcriptase activity autonomously within the cytoplasm [24]. Overexpression of RT domain resulted
191 in elevated levels of cytoplasmic RNA-DNA hybrids, consistent with recent findings reported by
192 Kathleen's group [24], as evidenced by increased s9.6 signals in the IF experiments **(Figure** 3A**)**. This
193 was accompanied by elevated transcript levels of DNA damage indicators (RAD51, BRCA1, and Rb)
194 and inflammatory markers (IL6, STING pathway, IRF-7, MCP-1, CXCL-10, IFN-β, and ISG-15)
195 measured using the qRT-PCR experiments **(Figure** 3B**)**. Upon 3TC treatment, the augmented RNA-
196 DNA hybrids in $p53^{-/-}$ overexpressing ORF1p-GFP, EN-GFP, and RT-GFP were mitigated **(Figure**
197 3A'**),** confirming the involvement of L1cDNA in RNA-DNA hybrid formation. This was corroborated
198 by decrease in accumulation of RAD51, BRCA1, RB and inflammatory gene markers **(Figure** 3B**)**
199 suggesting the aberrant formation of L1mRNA-cDNA with adverse effects on genome stability.
200 Moreover, to confirm if the overexpression of the RT-GFP leads to the generation of L1 trans R-
201 loops, we conducted sequential DRIP-qPCR experiments (**Figure** 3C). These experiments involved
202 immunoprecipitation using GFP from the *in vivo* RNH-GFP expressing $p53^{-/-}$ followed by the IP with
203 s9.6 antibodies to capture R-loops. This sequential immunoprecipitation assays validated that RT
204 domain alone can specifically facilitate the formation of R-loops in $p53^{-/-}$. Following this, IF assays
205 utilizing the yH2AX antibody demonstrated increased DNA damage in cells with the overexpression
206 of the RT domain **(Figures** 3D and D'**)** suggesting that the RT domain alone is capable of inducing
207 L1cDNA potentially culminating in the formation of L1trans R-loops derived RNA-DNA hybrids and
208 subsequent DNA damage.
209
210 **p53 promotes establishment of L1 re-silencing**
211 Given our findings that delineate the involvement of p53 in maintaining repression of L1 RNA-DNA
212 hybrids, we sought to investigate its potential involvement in facilitating the re-establishment of L1
213 silencing. To assess whether p53 is capable of restoring the silencing of previously activated L1
214 transposons, we employed HDACi drugs; TSA and NaB to induce L1 activation in a reporter system
215 where 5'UTR-egfp of L1 is inserted at the huAAVS1 site in both p53 wt and $p53^{-/-}$ cells of U2OS
216 **(Figures** 4A-F**)** and A375 **(Figures** S2A-G**)** [5]. Following a 24-hour treatment with HDACi drug (Figure
217 4A), the activation of L1 reporters were assessed by quantifying the GFP positive cells by comparing

218 the DMSO and 24h TSA panels using the confocal microscopy. The efficacy of both wt and p53$^{-/-}$
219 cells to suppress L1-5'UTR-eGFP upon drug withdrawal of 3 and 6 days elucidated a complete
220 silencing of GFP in wt but not in p53$^{-/-}$cells, this can be observed by comparing the panels of cells
221 treated with DMSO and those observed at the 4 and 7 days **(Figure** B**).** Similarly, the expression
222 levels of egfp transcripts correlated with the increased GFP intensities in L1-5'UTR-eGFP reporter
223 cells in response to HDACi **(Figures** C and D**)**. This activation of GFP closely corresponded to the
224 activation of endogenous L1-ORF1, as demonstrated through RNA *in situ* hybridization using
225 stellaris probes **(Supplementary Table 2 for probe sequences) (Figure** 4B**).** Four days after the
226 withdrawal of TSA, the activity of the L1-5'UTR-eGFP reporter returned to normal levels in cells with
227 the p53 wt status, but not in cells with the p53$^{-/-}$ genotype. No variation was detected in cellular
228 proliferation using the cell glow titre test between wt and p53$^{-/-}$ A375 L1-5'UTR-eGFP reporter cells
229 cells following HDACi treatment **(Figure** S2A**)**. Similarly, using qRT-PCR and microscopy, the
230 reactivation of GFP and L1-ORF1 and subsequent re-silencing were also detected in A375 wt after
231 24 treatment with HDAC inhibitors followed by 4 days of withdrawal, but not in the p53$^{-/-}$ cells
232 **(Figures** S2B-E**)**. In line with previous research on HDACi treated embryonic stem cells [16], our
233 experimental model demonstrated that inhibiting HDAC with TSA led to hyperacetylation of histones
234 H3 and H4. This was evident from the increased signal observed in western blotting when probed
235 with antibodies targeting H3Ac and H4Ac in both U2OS L1-5'UTR-eGFP **(Figures** 4E and 4F**)** and
236 A375 L1-5'UTR-eGFP reporter cell lines **(Figures** S2F and S2G**)**.
237 Next to determine whether p53 also enables resilencing of retrotransposition activation, we
238 used a synthetic L1 designated 99-gfp-LRE3 retrotransposition indicator [46,47], using HDACi
239 treatment, similar experiment was conducted on the stably transfected parental wt and p53$^{-/-}$ U2OS
240 cells, schematic shown (**Figure** 6A). This indicator **Figure** 6B mimics retrotransposition cycle
241 generating all the L1 intermediate components allowing direct measurements of *de novo*
242 retrotransposition rates by visualising GFP positive cells (green cells). Consistent with the L1-5'UTR
243 reporter, we noted re-silencing of L1-retrotransposition in wt cells upon withdrawal experiments after
244 TSA and NaB treatments. Whereas no re-silencing was observed in p53$^{-/-}$ cells as quantified in
245 **(Figures** 6C- 6D'**)**.
246
247 **p53 promotes restoration of deposition of histone repressive marks at L1-5'UTR**
248 In a previous study, we demonstrated that p53 regulates L1 transposons by epigenetic mechanisms
249 [9]. To investigate whether p53 can facilitate the re-silencing of L1 by recruiting these marks, we
250 activated L1 transposons in both A375 wt and p53$^{-/-}$ L1-5'UTR-eGFP reporters, as demonstrated in
251 **Figure 6**. The quantification of histone repressive marks H3K9me3 and H3K27me3 was performed

252 with ChIP-qPCR studies using primer sets targeting the p53 binding site at the L1-5'UTR (**Figure**
253 6A). Upon treatment of cells with HDACi drug (NaB), L1 activation coincided with the depletion of
254 H3K9me3 **(Figure** 6B**)** and H3K27me3 **(Figure** 6C**)**, as well as the acquisition of H3K9Ac **(Figures**
255 6D**)** and H3K4me3 **(Figures** 6E**).** Further, the levels of H3K9 and H3K27 trimethylation reversed
256 back to the DMSO treated levels following a 4-day drug withdrawal experiment in the wt with a
257 concurrent decrease in H3K9Ac marks and H3K4me3. Notably, changes were not observed in $p53^{-}$
258 $^{/-}$ cells. Importantly, this alteration in chromatin marks closely correlated with the reversal of L1
259 induction observed in wt cells, providing the evidence that p53 initiates the re-silencing of activated
260 L1 transposons by promoting the recruitment of epigenetic repressive marks and removal of
261 activating marks **(Figures** 4, 6 and S2**)**.
262
263 **A LINE1 reverse transcriptase antagonist reverses DNA damage triggered by L1**
264 The findings depicted in **Figures** 4 and S2 demonstrate that p53 establishes the resilencing of L1-
265 transposons upon HDACi withdrawal by mediating the recruitment of epigenetic repressive and
266 inhibiting activating marks at L1-5'UTR. HDACi is shown to induce DNA double-strand breaks in
267 cancer cells [48]. Therefore, to investigate the involvement of p53 in the reversal of L1 retroelement-
268 induced DNA damage, we subjected U2OS wt and $p53^{-/-}$ cells to HDACi (**as shown in Figure** 7A)
269 (**as shown in Figure** S3), followed by exposure to either DMSO or 3TC. Previous study from us has
270 shown L1-mediated genomic rearrangement in early passages of $p53^{-/-}$ cells [4], and similarly, we
271 observed induction of L1-ORF1p derepression accompanied by DNA damage upon TSA treatment
272 in both the wt and $p53^{-/-}$ U2OS cells. The treatment of $p53^{-/-}$ cells with 3TC resulted in restoration of
273 L1-ORF1p expression to the vehicle (DMSO) treated level, accompanied by a notable decrease in
274 the number of 53BP-1 foci, which serve as an indicator of DNA damage **(Figure** 7A**)**. The repair of
275 DNA damage and suppression of inflammatory genes to their uninduced levels occurred promptly in
276 wt cells, while it was impaired in $p53^{-/-}$ cells. Similar results were observed in staining with γH2AX,
277 an additional marker of double-stranded DNA breaks. **(Supplemental Figure** S3 A and A'**)**.
278 Collectively, our findings suggest that p53 facilitates the suppression of activated L1 transposons
279 that trigger DNA damage and inflammation. The immunofluorescence experiments on cells treated
280 with DMSO and NaB to evaluate the impact of HDACi on the acetylation and methylation levels of
281 H3K9 and H3K27 histones in both wt and $p53^{-/-}$ cells detected a global increase in the acetylation of
282 lysine residues on the H3 protein, notably at positions 9 and 27, accompanied by a reduction in
283 methylation at the same lysine residues **(Figures** S4 and S5**)**. Administering 3TC for 4 and 7 days
284 led to the reestablishment of these histone marks in normal cells, but not in cells lacking the p53
285 gene.

286 **Discussion**

287 Our comprehensive analyses, combining experimental and bioinformatic approaches, unveil the
288 pivotal function of p53 in repressing RNA-DNA hybrids originating from L1 R-loops encompassing
289 both the cis (L1mRNA-gDNA) and trans (L1mRNA-cDNA) configurations **(see Figures** 1 and 2**)**.
290 While previous studies primarily focused on the mutagenic potential of L1 *de novo* insertions, our
291 understanding of the impact of nucleic acid intermediates like L1 RNA-DNA hybrids and protein
292 products such as L1-ORF1p and ORF2p on genomic instability and inflammation remains limited.
293 Despite the relatively infrequent detection of new L1 insertions in cancer genomes compared to their
294 deleterious activity, L1 activation is a common feature in many sporadic cancer genomes, as
295 evidenced by recent pan-cancer studies [25,49,50]. Our finding regarding the prominent involvement of
296 L1 promoter in cis R-loop formation aligns with previous genome-wide studies highlighting the
297 enrichment of R-loops in promoter regions globally [41], supported by overlapping peaks of robust
298 DRIP-seq at the L1 promoter with those from the GRO-seq, indicating transcriptional pausing
299 generating cis RNA-DNA hybrids. Conversely, the implication of the L1-ORF2 genic region in trans
300 R-loop formation is substantiated by the diminished R-loop signals detected within the ORF2 region
301 subsequent to 3TC treatment in RNH-GFP expressing cells. **(Figure** 3**)**. R-loops are capable of
302 yielding both adverse and beneficial physiological outcomes in a cell [51], that prompted our
303 speculation that R-loops originating from retrotransposons could impede the finalization of
304 insertions—a critical controlling step in the retrotransposition process to prevent the amplification of
305 L1 copies in the genome. However, the observed decrease in DNA damage markers and
306 inflammation upon RT overexpression, coupled with a reduction in cytosolic RNA-DNA hybrids upon
307 treatment with 3TC in DRIP-qPCR and immunofluorescence assays, provides mechanistic insights
308 into the contribution of RNA-DNA-derived L1 R-loops to eliciting genome instability and inflammation,
309 the two hallmarks of cancer. This also indicates that, in addition to the canonical retrotransposition
310 insertion, other intermediate components can have oncogenic potential. These observations suggest
311 that L1 R-loops can act not only act as a bystander but act as a double edged sword in this context.

312 Furthermore, the inhibition of HDACs resulted in the loss of methylation and the gain of
313 acetylation at the 5'UTR, activating L1 and the derived R-loops (refer to **Figures** 3, 4, 5, and S2).
314 Withdrawal of HDACi caused permanent L1 derepression in $p53^{-/-}$ cells, inducing DNA damage and
315 inflammation triggered by L1 R-loop-derived RNA-DNA hybrids. In contrast, wild-type cells swiftly
316 silenced L1 by promoting H3K9me3 and H3K27me3 (**Figures** 6 and 7). This mechanism may confer
317 cancer resistance in p53-driven cancers treated with HDACi [52]. Additionally, treatment with 3TC
318 prevented the activation of L1 RNA-DNA hybrids representing the first evidence of trans L1 R-loop
319 formation in $p53^{-/-}$ unstressed cells as well as in HDACi-treated cells.

320 Our findings also suggest that p53 promotes the re-establishment of silencing of hyperactive
321 L1s, building upon our prior research showcasing the function of p53 in preserving L1 repression in
322 human somatic cell lines. Considering the function of p53 in mediating constitutive transcriptional
323 repression of L1s, and acknowledging the potential significance of R-loops, especially those
324 originating from nuclear L1mRNA-cDNAs, these discoveries could hold significant implications for
325 elucidating the mechanisms underlying p53 tumor suppression. Unlike conventional understandings,
326 this study reveals that the RT domain is involved in regulating RNA-DNA hybrids that triggers DNA
327 damage as seen in **Figure 3**. These unexplored oncogenic risks posed by the L1 RT domain trigger
328 acute inflammatory transcriptional programs upon overexpression, particularly in the absence of p53
329 [53-55]. Treatment with 3TC definitively prevented the induction of nearly all inflammatory genes and
330 DNA damage (**Figure 3)** in both wt and $p53^{-/-}$. Since 3TC is a potent inhibitor of the L1 reverse
331 transcriptase [56-58], these results indicate that L1 retrotransposition intermediates provoke
332 inflammatory programms in p53 deficient cells. Furthermore, these findings also suggest that the
333 induction of immune response genes may stem from the RT domain of ORF2p, attributed to the
334 cytosolic accumulation of RNA-DNA hybrids, along with the accumulation of trans L1 R-loops
335 assessed in sequential DRIP-qPCR assays on RNH-GFP *in vivo* system. Taken together, these
336 findings suggest that incorporating a reverse transcriptase inhibitor into personalized cancer therapy
337 [59] could enhance the efficacy of HDAC inhibitor treatment for cancer.
338
339 **Materials and Methods**
340 **Cell culturing:** p53 wild-type (wt) and p53 knockout ($p53^{-/-}$) cells of A375, U2OS cells were obtained
341 from Prof. John Abrams, UT Southwestern Medical Center, Dallas, Texas. A375 and U2OS cells
342 were cultured in Dulbecco's Modified Eagle's Medium (Gibco, #12100046). All cell lines were grown
343 at 37°C, 5% CO2 and passaged using Trypsin (Gibco, #15400054) in the presence of an anti-
344 antimycotic antibiotic (Gibco, #15240062) .
345
346 **Generation and screening of p53 knockout cells**
347 CRISPR cas9 editing (pX458), was used to generate $p53^{-/-}$ cell lines in the laboratory of Prof. John
348 Abrams at UTSW. $p53^{-/-}$ clones were identified by western blot using p53 monoclonal DO-1 (sc-
349 126) and L1-ORF1p expression levels were examined using anti L1-ORF1p antibody using
350 immunofluorescence experiments. Individual clones were grown until 100% confluent in 6-well plates
351 and whole cell lysates were prepared in RIPA lysis buffer (NaCl 140mM, EDTA 1uM, Tris HCl 10mM,
352 Triton X-100 1%, SDS 0.1%, Sodium Deoxycholate 0.1%) containing protease inhibitors (Roche).
353 Protein was quantified using Bradford assay (Protein Assay Kit, BioRad) and an equal amount of

354 total protein was loaded. Antibodies used were as follows: p53 monoclonal DO-1 (sc-126), anti L1-
355 ORF1p, clone4H1 (Millipore, #MABC1152) and β-actin (sigma, #A-2228). Sanger sequencing was
356 performed to confirm $p53^{-/-}$.
357
358 **Generation of huAAVS1 targeted L1-5'UTR-eGFP reporter cells**
359 The wt L1-5'UTR constructs, previously generated and kindly provided by Prof. John Abrams at
360 UTSW, were utilized. Stably transfected cells were created using huAAVS1-TALENL (Addgene
361 #59025) and huAAVS1-TALENR (Addgene #59026), along with donor plasmids. Three days after
362 transfection, single cells positive for GFP were sorted into 96-well plates using fluorescence-
363 activated cell sorting (FACS), following the protocol outlined in [4].
364
365 **For 3TC experiments**
366 2.5 x $10^5$ wt and $p53^{-/-}$ A375 and U2OS cells were plated into 6-well plates. After overnight of seeding
367 media was changed with fresh media containing DMSO, HDACi. After 24 h of HDACi treatment
368 media was replaced with fresh containing 3TC (10 μM). After 4 days and 7 days of 3TC treatment,
369 cells were harvested for RNA isolation or analysed for microscopy. qRT-PCR was conducted using
370 Applied Biosciences QuantStudio 5. Gene expression was normalized to β-actin, and fold induction
371 was calculated relative to the wild type. Primer sequences utilized in this study are available in
372 **Supplemental Table 1**.
373
374 **Real Time PCR experiments (RT-PCR)**
375 Total RNA was isolated using TRIzol (Invitrogen), then treated with Turbo DNase (Thermo Fischer,
376 #AM1907) for removal of DNA. RT-PCR was conducted utilizing cDNA synthesis kit Verso (Thermo
377 Fischer, #AB1453A). Applied biosciences Quant studio 5 was used for real time PCR and
378 normalization of gene expression was done against β-actin (for standard gene expression analysis),
379 RPL134 for DRIP-qPCR experiments, and fold induction was determined relative to the wild type.
380 Refer to Supplemental Table 1 for the primer sequences employed in RT-PCR assays.
381
382 **Effect of HDACi in wt and p53 cells expressing LRE3 retrotransposition**
383 2.5 x$10^5$ cells were transfected with equal amounts of 99-GFP-LRE3 (LRE3) plasmid, as previously
384 described [34]. After 72 h, cells were selected for puromycin resistance. Similar protocol was
385 followed for HDACi exposure followed by 3TC as mentioned in **Figure** 4. Confocal imaging was
386 performed using LSM780, at UTSW, Texas. GFP positive cells were counted from 5 images from
387 each of the samples. 2 biological replicates were performed.

388 **Statistical Analysis**

389 Quantitative data were collected from experiments conducted in at least two or three biological
390 replicates with technical replicates. One tailed Student's t-tests were calculated from three biological
391 replicates to detect statistically significant differences (with a cutoff of *$p<0.05$ and **$p<0.01$).

392

393 **Drug treatment**

394 TSA (Sigma Aldrich, #T8552) and NaB (Sigma Aldrich, #567430) were purchased Sigma. All drug
395 treatments were carried out in DMEM (Gibco, #12100046) supplemented with 10% (vol/vol) FBS
396 (Gibco, #A5256701) and 100X anti-antimycotic (Gibco, #15240062). Treatment with TSA (100nM)
397 was for 24 hr as indicated in the figure legend. NaB was used at 25 μM as indicated.

398

399 **Cloning of NLS tagged RNaseH1 with D210N**

400 For NLS-tagged RNaseH1D210N, cDNA fragments (purchased from IDT) [60] containing human
401 RNaseH1 with D210N catalytic dead mutant was amplified by PCR for cloning in pEGFP-N1 using
402 EcoRI (NEB, #R3101S) and KpnI (NEB, #R3142S) restriction sites. One SV40 nuclear localization
403 signal (NLS) (CCCAAAAAGAAACGCAAAGTG) was introduced by forward primer at the PCR step.
404 Primers used in PCR amplification are listed in **Supplemental Table 1**.

405

406 **Generation of stable cell lines expressing RNaseH1 D210N (RNH-GFP)**

407 To study R-loop in wt and $p53^{-/-}$ cells, nucleus localization sequences containing GFP-tagged,
408 catalytically-inactive RNase H1 D210N was cloned in pEGFN-1. The cloned sequence was verified
409 by sanger sequencing and A375 wt and $p53^{-/-}$ cells were transfected for the stable cell line generation
410 using G418 (Gibco, #11811064).

411

412 **ChIP-qPCR**

413 One billion A375 wt and $p53^{-/-}$ cells were grown in a 150 $cm^2$ dish and were fixed with 1%
414 formaldehyde in flasks at room temperature for 10 minutes and subsequently washed with ice-cold
415 PBS before a 125mM glycine solution was added to stop the fixation. The cells were scraped from
416 the flask and were resuspended in ChIP lysis buffer (50 mM HEPES-KOH pH7.5, 140 mM NaCl, one
417 mM EDTA pH8, 1% Triton X-100, 0.1% Sodium Deoxycholate, 0.1% SDS, Protease inhibitor). The
418 cell lysate was sonicated using an M220 Focused-ultrasonicator (Covaris) to release chromatin
419 lengths to 400bp, peak power 75.0, Duty factor =10, cycles/Burst =200, for 240 seconds. Chromatin
420 was diluted ten times with RIPA buffer and incubated with the following antibodies – H3K9me3 (Cell
421 Signalling Technologies #13969), H3K27me3 (Cell Signalling Technologies, #9733), H3K9Ac (Cell

422 Signalling Technologies, #9649) . Parallel protein A/G beads (EMD Millipore, #IP0515ML), H3K4Me
423 (Cell Signalling Technologies, #9751) were charged and incubated with the antibodies overnight,
424 following high salt, low salt, and LiCl washes the next day and eluted. Eluted chromatin was treated
425 with RNAase A (Thermo Fischer, #12091021) and proteinase K (NEB, #P8107S), crosslinks were
426 reversed, and samples were purified using a PCR purification kit (Qiagen). ChIP enrichment was
427 quantified by qPCR with Quant Studio 5 (Applied Biosciences).
428
429 **DRIP-qPCR**
430 One billion A375 p53 wt and p53$^{-/-}$ cells or cells expressing RNH mutant were plated into a 150 cm$^2$
431 dish for overnight (Tarsons) and were fixed by 1% formaldehyde, followed by quenching via Glycine
432 to a final concentration of 125 mM. Cells were rinsed twice with 10 mL cold PBS. 5 mL of cold PBS
433 was added, dishes were scraped thoroughly with a cell scraper and transferred. Cells were lysed in
434 750 ul lysis buffer composed of 140 mM NaCl, 1 mM EDTA (pH8),1% Triton X-100, 0.1% Sodium
435 Deoxycholate,0.1% SDS, Protease Inhibitors (added fresh each time) per 10 million cells. Cell lysis
436 was performed at room temperature. The cell lysate was sonicated to shear DNA to an average
437 fragment size of 400 bp by the M220 Ultrasonicator (Covaris) as previously mentioned for
438 ChIP**.** Approximately 25 µg of RNA-DNA hybrid per IP was used. Each sample was diluted 1:10 with
439 RIPA Buffer (50 mM Tris-HCl, pH8,150 mM NaCl, two mM EDTA pH8, 1% NP-40, 0.5% Sodium
440 Deoxycholate, 0.1% SDS, Protease Inhibitors (added fresh each time). Primary antibody RNA-DNA
441 hybrid (s9.6) antibody (Merck Millipore, #MABE1095, 3ul) or GFP (Thermo Fisher, 5ul) was added
442 to all samples and incubated at 4°C for 2 h. 60 ul of Pierce A/G Agarose beads were taken for 25 ug
443 of RNA-DNA hybrid. Beads were charged and incubated with the antibody incubated sample at 4
444 degrees overnight in shaking. The immunoprecipitated samples were washed by low salt, high salt,
445 and LiCl wash buffers. RNA-DNA hybrids were eluted by slowly adding 120 µL of elution buffer (1%
446 SDS, 100mM NaHCO3) to the protein A/G beads and vortex for 15 min at 30°C. 4.8 µL of 5 M NaCl
447 and 2 µL RNase A (10 mg/mL) were added and incubated while shaking at 65°C overnight. 2 µL
448 proteinase K (20 mg/mL) was added and incubated while shaking at 60°C for one hour. The RNA-
449 DNA hybrids were purified using a PCR purification kit (QIAGEN). Analysis of RNA-DNA hybrid level
450 was performed by qPCR.

451

452 **Quantification of RNA-DNA hybrids.**
453 RNA-DNA Hybrid levels were measured by RT-PCR using 2X POWER UP SYBR Green (Invitrogen,
454 #A25741) and analyzed via the QuantStudio 5 Real-Time PCR System (Applied Biosciences).

455 Primer sequences are listed in **Supplemental Table S1**. The qPCR results were analysed using the
456 percentage input method. The RNA-DNA hybrid enrichment was calculated based on the IP/Input
457 ratio. Three biological replicates were performed. The result is the average of all the biological
458 replicates.
459
460 **Immunofluorescence**
461 A375 p53 wt and p53$^{-/-}$ cells were cultured on poly-L-lysine (Sigma, #P4707)-coated coverslips,
462 washed with PBS and fixed with 4% paraformaldehyde. The cells were treated with 0.1% Triton X-
463 100 in PBS and 10% fetal bovine serum and were subsequently incubated with primary antibodies
464 at room temperature for 1 hour or 4 degrees overnight. After washing, secondary antibodies were
465 added and incubated in the dark at room temperature for 1 hour. Cells were washed with PBS and
466 counterstained with DAPI before observation under an Apotome microscope (Zeiss). All images were
467 taken using the same microscope parameters, and fluorescence quantification was performed using
468 fiji J software. Primary antibodies used were LINE1 ORF1p (Merck Milipore, #MABC1152), Anti
469 RNA-DNA Hybrid antibody (Merck Milipore, #MABE1095), yH2AX (Invitrogen, #MA1-2022),
470 H3K9me3 (Cell Signaling Technologies, #13969), H3K27me3 (Cell Signaling Technologies, #9733),
471 H3K9Ac (Cell Signaling Technologies, #9649), and 53BP1 (Cell Signaling Technologies, #4937), all
472 at a dilution of 1:50. Secondary antibodies used were: anti-mouse 568 (Thermo Fischer, #A-11031),
473 anti-mouse 488 (Thermo Fischer,#A-10680), anti-rabbit 488 (Thermo Fischer, #A-11008), and anti-
474 rabbit 568 (Thermo Fisher, #A-11011), at a dilution of 1:1000.
475
476 **Microscopy**
477 Images were captured using 60x oil objective Zeiss LSM780, LSM880 (UT Southwestern Medical
478 Center, Dallas, Texas) and Leica sp8 (ILS Bhubaneswar BT/INF/22/SP28293/2018) confocal
479 microscope. Zeiss Apotome 3 fluorescent microscope (IISER Berhampur) was also instrumental for
480 imaging. All images were processed via Fiji software package.
481
482 **Cytotoxicity assay using cell glow titre assay**
483 A total of 5000 A375 wt-5'UTR and p53$^{-/-}$ -5'UTR cells were distributed evenly into 96 well plates,
484 with each well containing either DMSO or a solution of NaB or TSA followed by 3TC. The CellTiter-
485 GLO kit from Promega (G7570) was utilized. Cells were treated with HDACi for 24, 48 or 72 h. 25 ul
486 of CellTiter-Glo® Reagent was added and mixed thoroughly for 2 minutes using an orbital shaker.
487 The plate was kept at room temperature for 10 minutes and the luminous signals were quantified

488 using a plate reader after 24, 48 and 72 h of treatment as per the instructions. Results are quantified
489 in relation to the DMSO control for each genotype.
490
491 **RNA *in situ* hybridization assays**
492 LGC Biosearch Technologies' Stellaris® RNA FISH Probe Designer was used for the designing of
493 Qusar-568 probes for L1-ORF1 probes, for RNA *in situ* hybridization. Protocol was followed as per
494 the manufacturer's instructions.
495
496 **Dataset Analyses**
497 DRIP-seq data of various cell lines (PMID 26579211), were retrieved from the NCBI Gene
498 Expression Omnibus (GEO) in SRA format. Before analysis, the data underwent preprocessing to
499 remove adapters and low-quality bases. Subsequently, the cleaned reads were aligned to the
500 GRCh38 human reference genome assembly (hg38) using the STAR aligner (version 2.7.10a). To
501 identify regions enriched with potential R-loops, MACS3 (Model-based Analysis of ChIP-Seq)
502 (version 3.0.0) with the 'macs3 callpeak -t' option was employed, ensuring precise localization within
503 the genome. Additionally, RepeatMasker (version 4.1.6) was applied, utilizing the 'RepeatMasker -
504 engine rmblast' option, to mask retrotransposable elements and repetitive sequences, thereby
505 maintaining the integrity of subsequent analyses [61]. Expression levels of retrotransposable elements
506 were quantified from the alignment files generated by STAR, followed by normalization for library
507 size and transcript length. Heatmaps illustrating the expression patterns of retrotransposable
508 elements across different cell lines were generated using the R programming language, with
509 visualization facilitated by the gplots package. Visualization of peaks across the full length of LINE1
510 was achieved through the UCSC Genome Browser.74.
511
512 **Supplemental Information**
513 Supplemental Tables 2
514 Supplemental Figures 1-5
515
516 **Acknowledgements**
517 This work was supported by the DBT/Wellcome Trust India Alliance fellowship (IA/I/22/2/506501) to
518 Bhavana Tiwari, Pratyashaa Paul (IISER Berhampur), Arun Kumar (CSIR-JRF), Astik Kumar De
519 (UGC-JRF). The authors would also like to acknowledge the assistance of ILS Bhubaneswar
520 confocal imaging facility and the UTSW, Dallas, Texas for confocal imaging facility. We acknowledge
521 Prof. John Abrams at the Department of Cell Biology, University of Texas Southwestern Medical

522 Center, Texas for generously providing chemicals, research reagents, including wild-type and p53
523 knockout cells, as well as plasmid resources utilized in this study. We thank Dr. Amanda Jones and
524 Prof. John Abrams of UTSW, Texas for valuable suggestions. Illustration work for graphical abstract
525 was created with BioRender.com. We thank IISER Berhampur for the support.
526

527 **Contributions**

528 BT conceived the studies. PP, AK, AKD, AP, GP, FP and BT performed experiments and analysed
529 data. SK processed the microscopy data and assisted in the illustration of the graphical abstract. BT
530 designed the study, analysed data, and both BT and PP wrote the manuscript.
531

532 **Declaration of interests**

533 The authors declare no competing interests.
534

535 **Figure legends**
536

537 **Figure 1. Elevation of L1 encoded intermediate components in p53$^{-/-}$ cells:**
538 **(**A-B) qRT-PCR analyses was performed using the primers that detects consensus sequences of
539 5'UTR, L1ORF1 and L1ORF2 transcripts in wt and p53$^{-/-}$ of (A) A375 and (B) U2OS cells. The
540 transcript levels were normalized using ß-actin and relative fold change was calculated with respect
541 to the parental wild type. The data shown are the averages of three biological replicates. *$p<0.05$,
542 **$p<0.01$, (Mann-Whitney U test).

543 (C-D) Representative confocal images display immunofluorescence staining for L1-ORF1p (Alexa
544 Fluor 568, red) and DAPI (blue) in wt and p53$^{-/-}$ cells of (C) A375 and (D) U2OS. Scale bars, 100
545 µm and 30 µm respectively.

546 (E) Immunofluorescence images s9.6 stained (Alexa Fluor, 488) and DAPI (blue) A375 wt and p53$^{-}$
547 $^{/-}$ cells. Scale bar,100 µm. Shown images are representative of three biological replicates.

548 (E') Quantification of s9.6 intensities of whole cell from A375 p53 wt and p53$^{-/-}$ using fiji. Minimum 60
549 cells were analysed for RNA-DNA hybrid quantification from three biological replicates. *$p<0.05$,
550 ns=non-significant (Mann-Whitney U test).

551 (F) DRIP-qPCR was performed to measure R-loops in A375 p53 wt and p53$^{-/-}$ cells.
552 Immunoprecipitation carried out using the s9.6 antibody. Arrows at the schematic indicate to primers

553 amplifying different regions of L1 sequence at 5'-UTR, ORF1 and ORF2). RPL13A was used a
554 positive control for quantification of the R-loop locus and ZNF544 as negative locus. Enrichment of
555 RNA-DNA hybrids in each region, normalized to input values. Data represent mean± S.D. from three
556 biological experiments. *p<0.05, ns=non-significant (Mann-Whitney U test).

557 (G) The representative fluorescent images show A375 wt and $p53^{-/-}$ cells transfected with RNaseH1
558 D210N-GFP (RNH-GFP) construct. The nuclear foci indicate the expression of RNaseH1 D210N-
559 GFP (RNH-GFP, green), nucleus (Blue).

560 (H) DRIP-qPCR on RNaseH D210N-GFP stably transfected cells of A375 wt and $p53^{-/-}$ cells using
561 the primers detecting L1-5'UTR, ORF1 and ORF2 loci. RPL13A used as a positive control for the R-
562 loop enrichment and ZNF544 as negative locus. Signal values of RNA-DNA hybrids
563 immunoprecipitated in each region, normalized to input values. Data represent mean±S.D. from the
564 three independent experiments. *p<0.05, ns=non-significant (Mann-Whitney U test).

565 (I) This figure illustrates the comparison of DRIP-seq signals in the input control and
566 immunoprecipitated sample, as well as the GRO-seq signal from the same cell line. The analyses
567 from the dataset (PMID 26579211) focuses on a specific L1Hs genomic region. The green peak
568 corresponds to the input of DRIP-seq data, whereas the blue peaks reflects the DRIP-sequenced
569 data obtained from s9.6 immunoprecipitated HEK293T cells. The orange curve indicates Gro-seq
570 data from HEK293T cells to quantify nascent RNAs at L1. The depicted schematic shows the L1
571 regions: 5'UTR, ORF1, and ORF2 (represented by black bars). The data also provides insights on
572 the genomic locations of L1 in chromosome 7 of the hg38 assembly.

573

574 **Figure 2. Increased accumulation of L1 trans R-loops derived RNA-DNA hybrids in $p53^{-/-}$**
575 (A) Heat map shows R-loops enrichment in human TE families obtained from the DRIP-seq data
576 analysis. Each row represents a TE family grouped according to their repBase classification. The L1
577 has been classified as per their age, e.g. L1-young are full length sequences and are capable of
578 retrotransposition including the loci from L1Hs family. Rows are clustered using the K-means
579 algorithm and columns represent the sample types (with p53 status of the cells). The legend
580 represents the differential presence of various TE families in the sample. Adjusted p-value of the
581 Table is 0.05. Sample 1 (SRR2028291), 2 (SRR2028292), 3 (SRR5137197), 4 (SRR5137200), 5
582 (SRR2028293), 6 (SRR2028294), 7 (SRR9937575), 8 (SRR9937576).
583

584 (B) Illustration of strategies involving DMSO or NaB drug (25 µm) treatment on A375 wt and p53$^{-/-}$,
585 as indicated for 24 hours, followed by drug withdrawal for 4 and 7 days. Cell viability was assessed
586 through cell glow titre experiments at (1 day, 3 days and 7 of drug treatment) (**Supplemental Figure**
587 **S3A**) to measure HDACi drug toxicity.
588
589 (C) Full-length L1 transcript analyses were performed in SW480 cell line (green) treated with NaB
590 and from human pancreatic islets (HPI, yellow) treated with TSA (PMID: 38410440, 38410440).
591 (Mann-Whitney U Test, *p<0.05). These cell lines are reported to harbour p53 mutation.
592
593 (D) qRT-PCR analysis of L1 ORF1 (green) expression of A375 wt and p53$^{-/-}$ upon NaB treatment.
594 The data shown are the averages of three biological replicates (Mann-Whitney U Test, *p<0.05,
595 **p<0.01).
596
597 (D) qRT-PCR analysis of L1 ORF1 expression of A375 wt and p53$^{-/-}$ upon NaB treatment. The data
598 shown are the averages of three biological replicates (Mann-Whitney U Test, *p<0.05, **p<0.01).
599
600 (E) Representative immunofluorescence microscopy images of three biological replicates showing
601 RNA-DNA hybrid accumulation in wt and p53$^{-/-}$ A375 cells after treatment with either DMSO or NaB
602 for 24 hours, followed by 3TC treatment for 72 hours. Scale bar indicates 50 um.
603
604 (E') Quantification of s9.6 intensities from the whole cells was done using Fiji software [62]. Violin plots
605 exhibit combined data from three biological replicates with p values determined by Mann–Whitney
606 test. p<0.05,*p<0.01. A minimum of 50 cells were measured in each sample of the three biological
607 replicates.
608
609 (F) DRIP-qPCR was performed to measure R-loops in A375 p53 wt and p53$^{-/-}$ cells upon 3TC
610 treatment. Immunoprecipitation carried out using the s9.6 antibody. Enrichment of RNA-DNA hybrids
611 in each region, normalized to input values. Data represent mean±S.D. from three independent
612 experiments. *p<0.05, ns=non-significant (Mann-Whitney U test).
613
614 (G) DRIP-qPCR on RNaseH D210N-GFP stably transfected cells of A375 p53 wt and p53$^{-/-}$ cells
615 upon 3TC treatment. Immunoprecipitation carried out using the GFP antibody. Enrichment of RNA-
616 DNA hybrids in each region, normalized to input values. Data represent mean±S.D. from three
617 independent experiments. *p<0.05, ns = non-significant (Mann-Whitney U test).

618 **Figure 3. Effect of reverse transcriptase inhibitor on RT domain overexpressing p53$^{-/-}$ cells**
619 (A) Representative fluorescence images depict the transient overexpression of A375 p53$^{-/-}$ cells with
620 pEGFP-N1 (EV), L1-ORF1p, Endonuclease (EN), Reverse Transcriptase (RT) domains of L1-
621 ORF2p followed by 3TC treatment for 3 days post transfection of 24 h. The overexpressed proteins
622 are c-terminally GFP tagged (green) and s9.6 (red) that visualize RNA-DNA hybrids are mostly
623 localised at the cytoplasm, nucleus is stained with DAPI (blue). Scale bar represents 50um.
624
625 (B) The heatmap shows a consolidated qRT-PCR of DNA repair genes (RAD50, BRCA1, Rb) and
626 inflammatory markers (STING, IRF7, MCP, CXCL10, IFNβ, ISG15) from the exogenously expressed
627 ORF1p, EN domain, RT domain in A375 p53$^{-/-}$ cells followed by 3TC treatment for 3 days. The
628 subsequent legend shows the level of expression following overexpression. The samples were
629 harvested after 3TC treatment for 3 days on 24 h transfected cells. The data from three biological
630 replicates were included for heatmap generation. The normalised p-value of the data is less than
631 0.05.
632
633 (C) Sequential DRIP-qPCR was performed on RT-GFP exogenously overexpressing A375 p53$^{-/-}$
634 followed by DMSO or 3TC treatment for 3 days. The first round of immunoprecipitation was
635 performed using GFP antibody followed by another round of immunoprecipitation by s9.6 on the
636 GFP immunoprecipitated samples. Enrichment of RNA-DNA hybrids in each sample, normalized to
637 the respective input values. Data represent mean±S.D. from the three independent experiments.
638
639 (D) Representative confocal images of EV, EN, RT (all GFP tagged) transiently overexpressing p53$^{-}$
640 $^{/-}$ cells (green) and yH2AX foci (red) localised at the nucleus (DAPI, blue). The merged images show
641 overlap of yH2AX , DAPI , GFP. Scale bar represents 50um.
642
643 (D') Violin plots represent the y2AX (red) foci quantification. yH2AX foci were quantified via Fiji
644 software. The mean (black line) represent the average foci from 50 nuclei. The data was quantified
645 using fiji between three biological replicates. *$p<0.05$ (Mann-Whitney U test).
646
647 **Figure 4. The dynamics of the L1-5'UTR-eGFP reporter upon exposure to HDAC inhibitors**
648 **and subsequent drug withdrawal.**
649 (A) Illustrates the schematic of TSA drug treatment and withdrawal in U2OS wt and p53$^{-/-}$ cells. The samples
650 were collected for qRT-PCR, western blotting, and microscopy at 24 hours post-drug (HDACi) treatment, as
651 well as at 4 and 7 days. TSA and NaB denote drug treatment for 24 hours, TSA-4D and NaB-4D indicate

652 drug withdrawal of 3 days, and TSA-7D and NaB-7D signify withdrawal after 6 days post 24-hour treatment
653 (L1-ORF1; 568, GFP; 488, and DAPI channels).
654
655 (B) Confocal imaging of GFP and RNA *in situ* hybridization of L1-ORF1 using Stellaris probes (from
656 LGC Biosearch Technologies) was performed in wt and p53$^{-/-}$ U2OS cells harbouring L1-5'UTR-
657 eGFP construct. The reporter cells were treated with either DMSO or TSA for 24 hours, followed by
658 withdrawal for 3 and 6 days. Samples were collected at 1 day, 4 days, and 7 days for confocal
659 imaging post HDACi treatment for GFP activation and silencing. Presented here are representative
660 confocal images from three independent immunofluorescence experiments. Activation of L1-ORF1
661 transcripts was visualised using Qusar 570 Stellaris probes sequences (**Supplementary Table 2**).
662 Scale bar indicates 20 um.
663
664 (C-D) RT-qPCR analysis was performed to quantify L1-ORF1 and gfp transcripts in wt and p53$^{-/-}$ L1-
665 5'UTR cells treated with DMSO or TSA/NaB at 1, 4 and 7 days. The data represent the mean ±
666 standard deviation (S.D.) from three independent biological replicates (n=3). *$p<0.05$, **$p<0.01$,
667 ns=non-significant. (Mann-Whitney U test). The primers used for qPCR analysis of ORF1 and egfp
668 transcripts are provided in **Supplemental Table 1.**
669
670 (E-F) Western blotting of H3Ac and total H3 levels (E) and H4Ac and H4 total levels (F) in U2OS wt
671 and p53$^{-/-}$ cells upon either DMSO or TSA 24 h treatment.
672
673 **Figure 5. p53 facilitates the rapid re-establishment of LRE3 silencing, a retrotransposition**
674 **indicator, following withdrawal of HDACi drugs.**
675 (A) Illustrates the schematic representation of DMSO, TSA/NaB drug treatment and subsequent
676 withdrawal in U2OS wt and p53$^{-/-}$ cells.
677
678 (B) Illustrations indicates the nature of LRE3 plasmid which is a surrogate marker of
679 retrotransposition. Cells that undergo retrotransposition are GFP positive (green).
680
681 (C-D) The representative confocal images demonstrate the expression of GFP (green) in U2OS wt
682 and p53$^{-/-}$ cells following exposure to TSA (C) and NaB (D) drugs for 24 hours, followed by drug
683 withdrawal of 3 or 6 days. Scale bar indicates 20um and the experiments were conducted with 3
684 biological replicates.

685 (C'-D') Percentage of GFP positive cells in U2OS wt and p53$^{-/-}$ at 24 hrs of TSA (C) and NaB (D)
686 treatment followed by drug withdrawal at 3 and 6 days. GFP positive cells were counted from
687 minimum 10 fields from the 3 independent experiments. The error bar represents mean of 3
688 biological replicates. *p<0.05, **p<0.01, ns=non-significant (Mann-Whitney U test).
689
690 **Figures 6. Histone modification dynamics in L1-5'UTR-eGFP reporter cells upon HDACi**
691 **exposure and withdrawal**
692 (A-C) Chromatin immunoprecipitation followed by qPCR analyses was conducted on the 5'UTR
693 region of A375 wt and p53$^{-/-}$ L1-5'UTR-eGFP stable cells. Primers targeting the p53 binding region
694 were utilized, with immunoprecipitation carried out using antibodies against histone modifications
695 H3K9me3, H3K27me3, H3K9Ac, and H3K4me3. The results illustrate normalized levels of H3K9me3
696 and H3K27me3, representative of repressive histone marks (A and B), normalized to input values,
697 as well as levels of activation marks H3K9Ac (C) and H3K4me3 (D). Reporter cells were treated with
698 HDACi for 24 h followed by withdrawal for 3 and 6 days. Samples for analyses were collected at 1
699 day, 4 and 7 days (for drug withdrawal), as depicted (refer to **Figures** 4 and 5). It is noteworthy that
700 alterations in H3K9me3, H3K27me3, H3K9Ac, and H3K4me3 enrichment are specific to the p53
701 status. Error bars represent the standard error of the mean from three biological replicates. *p<0.05,
702 **p<0.01, ns=non-significant (Mann-Whitney U test).
703
704 **Figure 7. Effect of 3TC on L1-ORF1p expression and 53BP-1 foci**
705 (A) Confocal imaging of L1-ORF1p (green), 53BP-1 (magenta, foci indicated in white) and nucleus
706 (blue) in U2OS wt and lacking p53 were treated with either DMSO or TSA for 24 hours, followed by
707 3TC treatment for 3 and 6 days. Imaging of cells performed at 1 day after TSA exposure, and at 3
708 and 6 days after 3TC treatment. Presented here are representative confocal images from three
709 independent immunofluorescence imaging experiments. Upon 24-hour exposure to TSA, activation
710 of L1-ORF1p and accumulation of 53BP-1 foci (indicated by white arrows) were observed.
711 Conversely, suppression of L1-ORF1p and reduction of 53BP-1 foci were more evident in wt than
712 p53$^{-/-}$ cells after 3 and 6 days of 3TC treatment. Scale bar denotes 20um.
713
714 (A') The Violin plot shows the quantified 53BP1 foci from microscopy images. The bold dotted line
715 represent the mean foci from 50 different nuclei. The quantification has been done from 3 different
716 biological replicates. *p<0.05, ns=non-significant (Mann-Whitney U test).
717
718

## References


1. Soussi, T., and Wiman, K.G. (2015). TP53: an oncogene in disguise. Cell death and differentiation *22*, 1239-1249. 10.1038/cdd.2015.53.
2. Vousden, K.H., and Lane, D.P. (2007). p53 in health and disease. Nat Rev Mol Cell Biol *8*, 275-283. 10.1038/nrm2147.
3. McKerrow, W., Wang, X., Mendez-Dorantes, C., Mita, P., Cao, S., Grivainis, M., Ding, L., LaCava, J., Burns, K.H., Boeke, J.D., and Fenyo, D. (2022). LINE-1 expression in cancer correlates with p53 mutation, copy number alteration, and S phase checkpoint. Proc Natl Acad Sci U S A *119*. 10.1073/pnas.2115999119.
4. Tiwari, B., Jones, A.E., Caillet, C.J., Das, S., Royer, S.K., and Abrams, J.M. (2020). p53 directly represses human LINE1 transposons. Genes Dev. 10.1101/gad.343186.120.
5. Rodriguez-Martin, B., Alvarez, E.G., Baez-Ortega, A., Zamora, J., Supek, F., Demeulemeester, J., Santamarina, M., Ju, Y.S., Temes, J., Garcia-Souto, D., et al. (2020). Pan-cancer analysis of whole genomes identifies driver rearrangements promoted by LINE-1 retrotransposition. Nat Genet *52*, 306-319. 10.1038/s41588-019-0562-0.
6. Shin, Y.J., Kim, Y., Wen, X., Cho, N.Y., Lee, S., Kim, W.H., and Kang, G.H. (2019). Prognostic implications and interaction of L1 methylation and p53 expression statuses in advanced gastric cancer. Clin Epigenetics *11*, 77. 10.1186/s13148-019-0661-x.
7. Wylie, A., Jones, A.E., D'Brot, A., Lu, W.J., Kurtz, P., Moran, J.V., Rakheja, D., Chen, K.S., Hammer, R.E., Comerford, S.A., et al. (2016). p53 genes function to restrain mobile elements. Genes Dev *30*, 64-77. 10.1101/gad.266098.115.
8. Tiwari, B., Kurtz, P., Jones, A.E., Wylie, A., Amatruda, J.F., Boggupalli, D.P., Gonsalvez, G.B., and Abrams, J.M. (2017). Retrotransposons Mimic Germ Plasm Determinants to Promote Transgenerational Inheritance. Curr Biol *27*, 3010-3016 e3013. 10.1016/j.cub.2017.08.036.
9. Tiwari, B., Jones, A.E., Caillet, C.J., Das, S., Royer, S.K., and Abrams, J.M. (2020). p53 directly represses human LINE1 transposons. Genes Dev *34*, 1439-1451. 10.1101/gad.343186.120.
10. Tiwari, B., Jones, A.E., and Abrams, J.M. (2018). Transposons, p53 and Genome Security. Trends Genet *34*, 846-855. 10.1016/j.tig.2018.08.003.
11. Harris, C.R., Dewan, A., Zupnick, A., Normart, R., Gabriel, A., Prives, C., Levine, A.J., and Hoh, J. (2009). p53 responsive elements in human retrotransposons. Oncogene *28*, 3857-3865. 10.1038/onc.2009.246.

752 12. Zemojtel, T., Kielbasa, S.M., Arndt, P.F., Chung, H.R., and Vingron, M. (2009). Methylation
753 and deamination of CpGs generate p53-binding sites on a genomic scale. Trends Genet *25*,
754 63-66. 10.1016/j.tig.2008.11.005.
755 13. Cui, F., Sirotin, M.V., and Zhurkin, V.B. (2011). Impact of Alu repeats on the evolution of
756 human p53 binding sites. Biol Direct *6*, 2. 10.1186/1745-6150-6-2.
757 14. Ardeljan, D., Taylor, M.S., Ting, D.T., and Burns, K.H. (2017). The Human Long Interspersed
758 Element-1 Retrotransposon: An Emerging Biomarker of Neoplasia. Clin Chem *63*, 816-822.
759 10.1373/clinchem.2016.257444.
760 15. Burns, K.H. (2017). Transposable elements in cancer. Nat Rev Cancer *17*, 415-424.
761 10.1038/nrc.2017.35.
762 16. Brunmeir, R., Lagger, S., Simboeck, E., Sawicka, A., Egger, G., Hagelkruys, A., Zhang, Y.,
763 Matthias, P., Miller, W.J., and Seiser, C. (2010). Epigenetic regulation of a murine
764 retrotransposon by a dual histone modification mark. PLoS Genet *6*, e1000927.
765 10.1371/journal.pgen.1000927.
766 17. Garcia-Perez, J.L., Morell, M., Scheys, J.O., Kulpa, D.A., Morell, S., Carter, C.C., Hammer,
767 G.D., Collins, K.L., O'Shea, K.S., Menendez, P., and Moran, J.V. (2010). Epigenetic silencing
768 of engineered L1 retrotransposition events in human embryonic carcinoma cells. Nature *466*,
769 769-773. 10.1038/nature09209.
770 18. Gaillard, S.L., Zahurak, M., Sharma, A., Durham, J.N., Reiss, K.A., Sartorius-Mergenthaler,
771 S., Downs, M., Anders, N.M., Ahuja, N., Rudek, M.A., and Azad, N. (2019). A phase 1 trial of
772 the oral DNA methyltransferase inhibitor CC-486 and the histone deacetylase inhibitor
773 romidepsin in advanced solid tumors. Cancer *125*, 2837-2845. 10.1002/cncr.32138.
774 19. Rodriguez-Martin, B., Alvarez, E.G., Baez-Ortega, A., Zamora, J., Supek, F.,
775 Demeulemeester, J., Santamarina, M., Ju, Y.S., Temes, J., Garcia-Souto, D., et al. (2020).
776 Pan-cancer analysis of whole genomes identifies driver rearrangements promoted by LINE-
777 1 retrotransposition. Nat Genet *52*, 306-319. 10.1038/s41588-019-0562-0.
778 20. Goodier, J.L. (2016). Restricting retrotransposons: a review. Mob DNA *7*, 16.
779 10.1186/s13100-016-0070-z.
780 21. Rodic, N., Sharma, R., Sharma, R., Zampella, J., Dai, L., Taylor, M.S., Hruban, R.H.,
781 Iacobuzio-Donahue, C.A., Maitra, A., Torbenson, M.S., et al. (2014). Long interspersed
782 element-1 protein expression is a hallmark of many human cancers. Am J Pathol *184*, 1280-
783 1286. 10.1016/j.ajpath.2014.01.007.
784 22. Crow, M.K. (2010). Long interspersed nuclear elements (LINE-1): potential triggers of
785 systemic autoimmune disease. Autoimmunity *43*, 7-16. 10.3109/08916930903374865.

786 23. Subbalekha, K., Pimkhaokham, A., Pavasant, P., Chindavijak, S., Phokaew, C.,
787 Shuangshoti, S., Matangkasombut, O., and Mutirangura, A. (2009). Detection of LINE-1s
788 hypomethylation in oral rinses of oral squamous cell carcinoma patients. Oral Oncol *45*, 184-
789 191. 10.1016/j.oraloncology.2008.05.002.
790 24. Baldwin, E.T., van Eeuwen, T., Hoyos, D., Zalevsky, A., Tchesnokov, E.P., Sanchez, R.,
791 Miller, B.D., Di Stefano, L.H., Ruiz, F.X., Hancock, M., et al. (2024). Structures, functions and
792 adaptations of the human LINE-1 ORF2 protein. Nature *626*, 194-206. 10.1038/s41586-023-
793 06947-z.
794 25. De Cecco, M., Ito, T., Petrashen, A.P., Elias, A.E., Skvir, N.J., Criscione, S.W., Caligiana, A.,
795 Brocculi, G., Adney, E.M., Boeke, J.D., et al. (2019). L1 drives IFN in senescent cells and
796 promotes age-associated inflammation. Nature *566*, 73-78. 10.1038/s41586-018-0784-9.
797 26. Gan, W., Guan, Z., Liu, J., Gui, T., Shen, K., Manley, J.L., and Li, X. (2011). R-loop-mediated
798 genomic instability is caused by impairment of replication fork progression. Genes Dev *25*,
799 2041-2056. 10.1101/gad.17010011.
800 27. Crossley, M.P., Bocek, M., and Cimprich, K.A. (2019). R-Loops as Cellular Regulators and
801 Genomic Threats. Molecular cell *73*, 398-411. 10.1016/j.molcel.2019.01.024.
802 28. Wells, J.P., White, J., and Stirling, P.C. (2019). R Loops and Their Composite Cancer
803 Connections. Trends Cancer *5*, 619-631. 10.1016/j.trecan.2019.08.006.
804 29. Stirling, P.C., Chan, Y.A., Minaker, S.W., Aristizabal, M.J., Barrett, I., Sipahimalani, P., Kobor,
805 M.S., and Hieter, P. (2012). R-loop-mediated genome instability in mRNA cleavage and
806 polyadenylation mutants. Genes Dev *26*, 163-175. 10.1101/gad.179721.111.
807 30. Wood, M., Quinet, A., Lin, Y.L., Davis, A.A., Pasero, P., Ayala, Y.M., and Vindigni, A. (2020).
808 TDP-43 dysfunction results in R-loop accumulation and DNA replication defects. J Cell Sci
809 *133*. 10.1242/jcs.244129.
810 31. Crossley, M.P., Song, C., Bocek, M.J., Choi, J.H., Kousouros, J.N., Sathirachinda, A., Lin,
811 C., Brickner, J.R., Bai, G., Lans, H., et al. (2023). R-loop-derived cytoplasmic RNA-DNA
812 hybrids activate an immune response. Nature *613*, 187-194. 10.1038/s41586-022-05545-9.
813 32. Dewannieux, M., Esnault, C., and Heidmann, T. (2003). LINE-mediated retrotransposition of
814 marked Alu sequences. Nat Genet *35*, 41-48. 10.1038/ng1223.
815 33. Kajikawa, M., and Okada, N. (2002). LINEs mobilize SINEs in the eel through a shared 3'
816 sequence. Cell *111*, 433-444. 10.1016/s0092-8674(02)01041-3.
817 34. Hancks, D.C., Goodier, J.L., Mandal, P.K., Cheung, L.E., and Kazazian, H.H., Jr. (2011).
818 Retrotransposition of marked SVA elements by human L1s in cultured cells. Hum Mol Genet
819 *20*, 3386-3400. 10.1093/hmg/ddr245.

820 35. Ostertag, E.M., Goodier, J.L., Zhang, Y., and Kazazian, H.H., Jr. (2003). SVA elements are
821 nonautonomous retrotransposons that cause disease in humans. Am J Hum Genet *73*, 1444-
822 1451. 10.1086/380207.
823 36. Anwar, S.L., Wulaningsih, W., and Lehmann, U. (2017). Transposable Elements in Human
824 Cancer: Causes and Consequences of Deregulation. Int J Mol Sci *18*.
825 10.3390/ijms18050974.
826 37. Imperatori, A., Sahnane, N., Rotolo, N., Franzi, F., Nardecchia, E., Libera, L., Romualdi, C.,
827 Cattoni, M., Sessa, F., Dominioni, L., and Furlan, D. (2017). LINE-1 hypomethylation is
828 associated to specific clinico-pathological features in Stage I non-small cell lung cancer. Lung
829 Cancer *108*, 83-89. 10.1016/j.lungcan.2017.03.003.
830 38. Briggs, E.M., Ha, S., Mita, P., Brittingham, G., Sciamanna, I., Spadafora, C., and Logan, S.K.
831 (2018). Long interspersed nuclear element-1 expression and retrotransposition in prostate
832 cancer cells. Mob DNA *9*, 1. 10.1186/s13100-017-0106-z.
833 39. Skourti-Stathaki, K. (2022). Detection of R-Loop Structures by Immunofluorescence Using
834 the S9.6 Monoclonal Antibody. Methods Mol Biol *2528*, 21-29. 10.1007/978-1-0716-2477-
835 7_2.
836 40. Sanz, L.A., and Chedin, F. (2019). High-resolution, strand-specific R-loop mapping via S9.6-
837 based DNA-RNA immunoprecipitation and high-throughput sequencing. Nat Protoc *14*,
838 1734-1755. 10.1038/s41596-019-0159-1.
839 41. Ginno, P.A., Lott, P.L., Christensen, H.C., Korf, I., and Chedin, F. (2012). R-loop formation is
840 a distinctive characteristic of unmethylated human CpG island promoters. Molecular cell *45*,
841 814-825. 10.1016/j.molcel.2012.01.017.
842 42. Lin, R., Zhong, X., Zhou, Y., Geng, H., Hu, Q., Huang, Z., Hu, J., Fu, X.D., Chen, L., and
843 Chen, J.Y. (2022). R-loopBase: a knowledgebase for genome-wide R-loop formation and
844 regulation. Nucleic Acids Res *50*, D303-D315. 10.1093/nar/gkab1103.
845 43. Yan, Q., Shields, E.J., Bonasio, R., and Sarma, K. (2019). Mapping Native R-Loops Genome-
846 wide Using a Targeted Nuclease Approach. Cell reports *29*, 1369-1380 e1365.
847 10.1016/j.celrep.2019.09.052.
848 44. Templeton, C.W., and Laimins, L.A. (2023). p53-dependent R-loop formation and HPV
849 pathogenesis. Proc Natl Acad Sci U S A *120*, e2305907120. 10.1073/pnas.2305907120.
850 45. Panatta, E., Butera, A., Mammarella, E., Pitolli, C., Mauriello, A., Leist, M., Knight, R.A.,
851 Melino, G., and Amelio, I. (2022). Metabolic regulation by p53 prevents R-loop-associated
852 genomic instability. Cell reports *41*, 111568. 10.1016/j.celrep.2022.111568.

853 46. Kopera, H.C., Larson, P.A., Moldovan, J.B., Richardson, S.R., Liu, Y., and Moran, J.V.
854 (2016). LINE-1 Cultured Cell Retrotransposition Assay. Methods Mol Biol *1400*, 139-156.
855 10.1007/978-1-4939-3372-3_10.
856 47. Ostertag, E.M., Prak, E.T., DeBerardinis, R.J., Moran, J.V., and Kazazian, H.H., Jr. (2000).
857 Determination of L1 retrotransposition kinetics in cultured cells. Nucleic Acids Res *28*, 1418-
858 1423. 10.1093/nar/28.6.1418.
859 48. Lee, J.H., Choy, M.L., Ngo, L., Foster, S.S., and Marks, P.A. (2010). Histone deacetylase
860 inhibitor induces DNA damage, which normal but not transformed cells can repair. Proc Natl
861 Acad Sci U S A *107*, 14639-14644. 10.1073/pnas.1008522107.
862 49. Rodriguez-Martin, B., Alvarez, E.G., Baez-Ortega, A., Zamora, J., Supek, F.,
863 Demeulemeester, J., Santamarina, M., Ju, Y.S., Temes, J., Garcia-Souto, D., et al. (2020).
864 Pan-cancer analysis of whole genomes identifies driver rearrangements promoted by LINE-
865 1 retrotransposition. Nat Genet. 10.1038/s41588-019-0562-0.
866 50. Simon, M., Van Meter, M., Ablaeva, J., Ke, Z., Gonzalez, R.S., Taguchi, T., De Cecco, M.,
867 Leonova, K.I., Kogan, V., Helfand, S.L., et al. (2019). LINE1 Derepression in Aged Wild-Type
868 and SIRT6-Deficient Mice Drives Inflammation. Cell Metab *29*, 871-885 e875.
869 10.1016/j.cmet.2019.02.014.
870 51. Hegazy, Y.A., Fernando, C.M., and Tran, E.J. (2020). The balancing act of R-loop biology:
871 The good, the bad, and the ugly. J Biol Chem *295*, 905-913. 10.1074/jbc.REV119.011353.
872 52. Hontecillas-Prieto, L., Flores-Campos, R., Silver, A., de Alava, E., Hajji, N., and Garcia-
873 Dominguez, D.J. (2020). Synergistic Enhancement of Cancer Therapy Using HDAC
874 Inhibitors: Opportunity for Clinical Trials. Front Genet *11*, 578011.
875 10.3389/fgene.2020.578011.
876 53. Bregnard, C., Guerra, J., Dejardin, S., Passalacqua, F., Benkirane, M., and Laguette, N.
877 (2016). Upregulated LINE-1 Activity in the Fanconi Anemia Cancer Susceptibility Syndrome
878 Leads to Spontaneous Pro-inflammatory Cytokine Production. EBioMedicine *8*, 184-194.
879 10.1016/j.ebiom.2016.05.005.
880 54. Saleh, A., Macia, A., and Muotri, A.R. (2019). Transposable Elements, Inflammation, and
881 Neurological Disease. Front Neurol *10*, 894. 10.3389/fneur.2019.00894.
882 55. Leonova, K.I., Brodsky, L., Lipchick, B., Pal, M., Novototskaya, L., Chenchik, A.A., Sen, G.C.,
883 Komarova, E.A., and Gudkov, A.V. (2013). p53 cooperates with DNA methylation and a
884 suicidal interferon response to maintain epigenetic silencing of repeats and noncoding RNAs.
885 Proc Natl Acad Sci U S A *110*, E89-98. 10.1073/pnas.1216922110.

886 56. Jones, R.B., Garrison, K.E., Wong, J.C., Duan, E.H., Nixon, D.F., and Ostrowski, M.A.
887 (2008). Nucleoside analogue reverse transcriptase inhibitors differentially inhibit human
888 LINE-1 retrotransposition. PLoS One *3*, e1547. 10.1371/journal.pone.0001547.
889 57. Dai, L., Huang, Q., and Boeke, J.D. (2011). Effect of reverse transcriptase inhibitors on LINE-
890 1 and Ty1 reverse transcriptase activities and on LINE-1 retrotransposition. BMC Biochem
891 *12*, 18. 10.1186/1471-2091-12-18.
892 58. Banuelos-Sanchez, G., Sanchez, L., Benitez-Guijarro, M., Sanchez-Carnerero, V., Salvador-
893 Palomeque, C., Tristan-Ramos, P., Benkaddour-Boumzaouad, M., Morell, S., Garcia-Puche,
894 J.L., Heras, S.R., et al. (2019). Synthesis and Characterization of Specific Reverse
895 Transcriptase Inhibitors for Mammalian LINE-1 Retrotransposons. Cell Chem Biol *26*, 1095-
896 1109 e1014. 10.1016/j.chembiol.2019.04.010.
897 59. Nishikawa, S., and Iwakuma, T. (2023). Drugs Targeting p53 Mutations with FDA Approval
898 and in Clinical Trials. Cancers (Basel) *15*. 10.3390/cancers15020429.
899 60. Crossley, M.P., Brickner, J.R., Song, C., Zar, S.M.T., Maw, S.S., Chedin, F., Tsai, M.S., and
900 Cimprich, K.A. (2021). Catalytically inactive, purified RNase H1: A specific and sensitive
901 probe for RNA-DNA hybrid imaging. J Cell Biol *220*. 10.1083/jcb.202101092.
902 61. Bao, W., Kojima, K.K., and Kohany, O. (2015). Repbase Update, a database of repetitive
903 elements in eukaryotic genomes. Mob DNA *6*, 11. 10.1186/s13100-015-0041-9.
904 62. Schindelin, J., Arganda-Carreras, I., Frise, E., Kaynig, V., Longair, M., Pietzsch, T., Preibisch,
905 S., Rueden, C., Saalfeld, S., Schmid, B., et al. (2012). Fiji: an open-source platform for
906 biological-image analysis. Nat Methods *9*, 676-682. 10.1038/nmeth.2019.
907

# Graphical Abstract

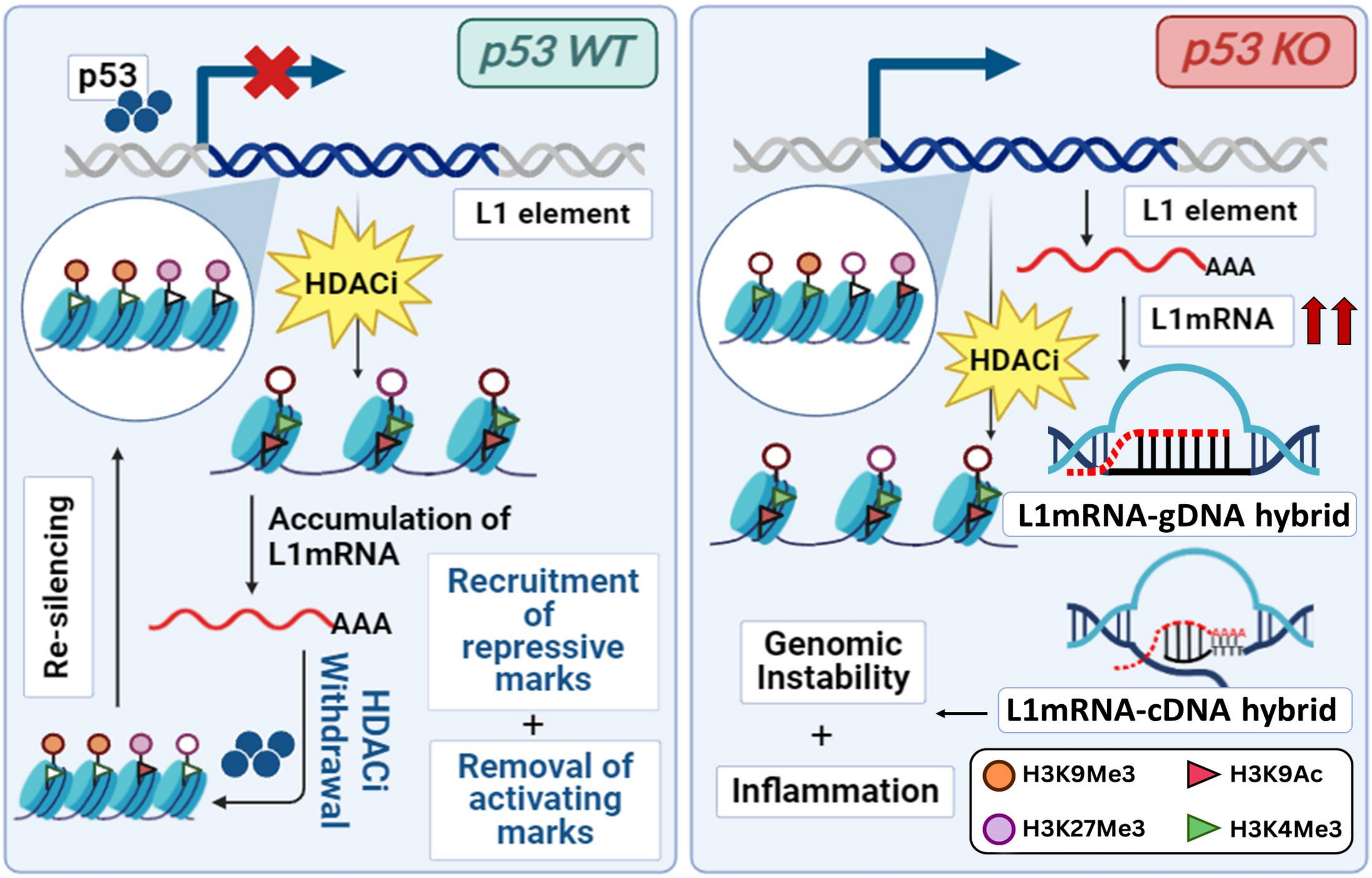

# Figure 1

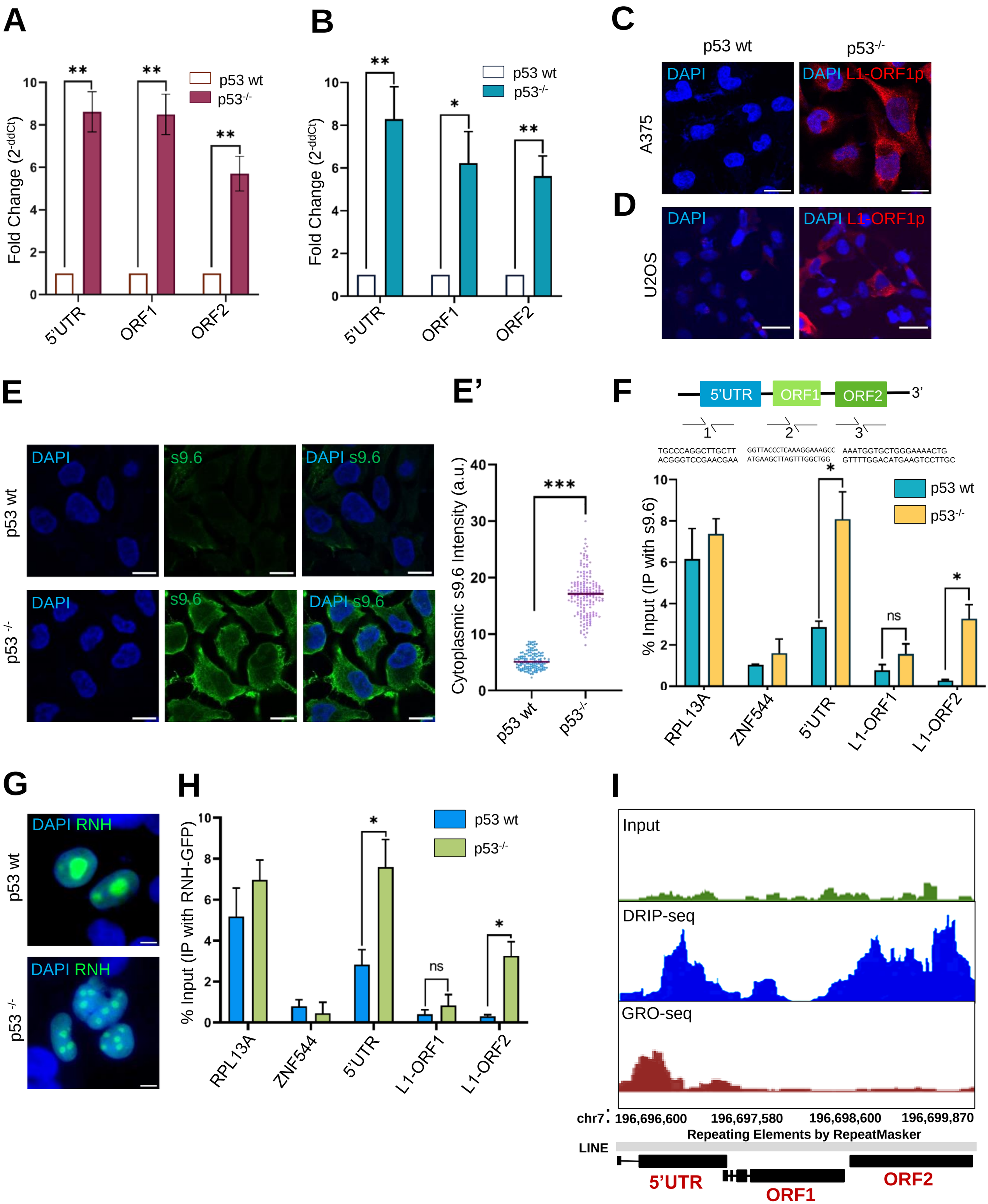
A
B
C
D
E
E'
F
G
H
I
p53 wt
p53-/-
Fold Change (2-ddCt)
5'UTR
ORF1
ORF2
A375
U2OS
DAPI
L1-ORF1p
s9.6
DAPI s9.6
Cytoplasmic s9.6 Intensity (a.u.)
TGCCCAGGCTTGCTT
ACGGGTCCGAACGAA
GGTTACCCTCAAAGGAAAGCC
ATGAAGCTTAGTTTGGCTGG
AAATGGTGCTGGGAAAACTG
GTTTTGGACATGAAGTCCTTGC
% Input (IP with s9.6)
RPL13A
ZNF544
L1-ORF1
L1-ORF2
ns
DAPI RNH
% Input (IP with RNH-GFP)
Input
DRIP-seq
GRO-seq
chr7:
196,696,600
196,697,580
196,698,600
196,699,870
Repeating Elements by RepeatMasker
LINE

# Figure 2

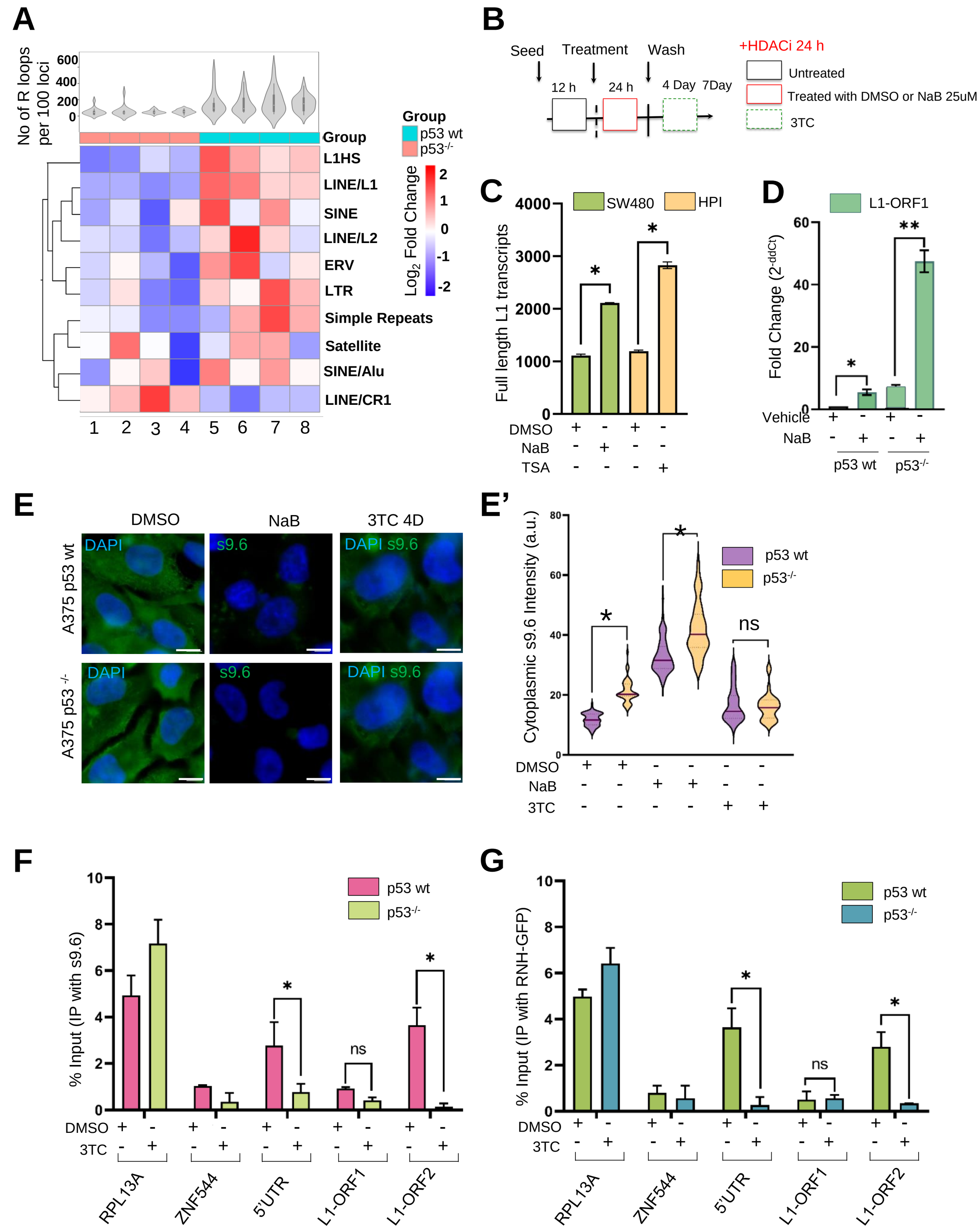
A
No of R loops per 100 loci
600
400
200
0
Group
L1HS
LINE/L1
SINE
LINE/L2
ERV
LTR
Simple Repeats
Satellite
SINE/Alu
LINE/CR1
1 2 3 4 5 6 7 8
Group
p53 wt
p53-/-
Log2 Fold Change
2
1
0
-1
-2
B
Seed
Treatment
Wash
12 h
24 h
4 Day
7Day
+HDACi 24 h
Untreated
Treated with DMSO or NaB 25uM
3TC
C
SW480
HPI
Full length L1 transcripts
4000
3000
2000
1000
0
DMSO + - + -
NaB - + - -
TSA - - - +
D
L1-ORF1
Fold Change (2-ddCt)
60
40
20
0
Vehicle + - + -
NaB - + - +
p53 wt
p53-/-
E
DMSO
NaB
3TC 4D
A375 p53 wt
A375 p53 -/-
DAPI
s9.6
DAPI s9.6
E'
Cytoplasmic s9.6 Intensity (a.u.)
80
60
40
20
0
p53 wt
p53-/-
ns
DMSO + + - - - -
NaB - - + + - -
3TC - - - - + +
F
% Input (IP with s9.6)
10
8
6
4
2
0
p53 wt
p53-/-
ns
DMSO + - + - + - + - + -
3TC - + - + - + - + - +
RPL13A
ZNF544
5'UTR
L1-ORF1
L1-ORF2
G
% Input (IP with RNH-GFP)
10
8
6
4
2
0
p53 wt
p53-/-
ns
DMSO + - + - + - + - + -
3TC - + - + - + - + - +
RPL13A
ZNF544
5'UTR
L1-ORF1
L1-ORF2

# Figure 3

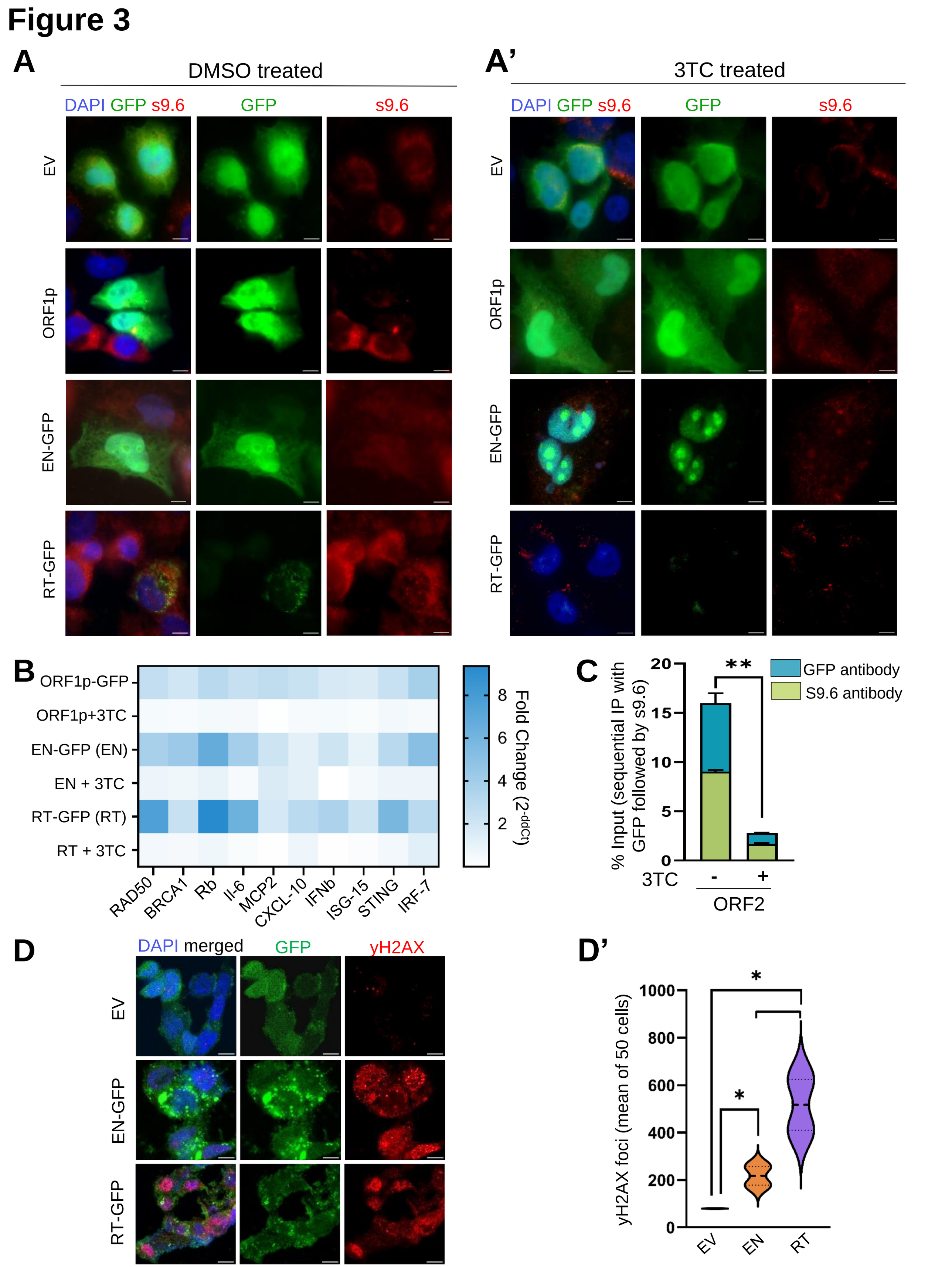
A
DMSO treated
DAPI GFP s9.6
GFP
s9.6
EV
ORF1p
EN-GFP
RT-GFP
A'
3TC treated
B
ORF1p-GFP
ORF1p+3TC
EN-GFP (EN)
EN + 3TC
RT-GFP (RT)
RT + 3TC
RAD50
BRCA1
Rb
Il-6
MCP2
CXCL-10
IFNb
ISG-15
STING
IRF-7
Fold Change (2-ddCt)
8
6
4
2
C
% Input (sequential IP with GFP followed by s9.6)
20
15
10
5
0
**
GFP antibody
S9.6 antibody
3TC
-
+
ORF2
D
DAPI merged
GFP
yH2AX
EV
EN-GFP
RT-GFP
D'
yH2AX foci (mean of 50 cells)
1000
800
600
400
200
0
*
*
EV
EN
RT

# Figure 4

**A**

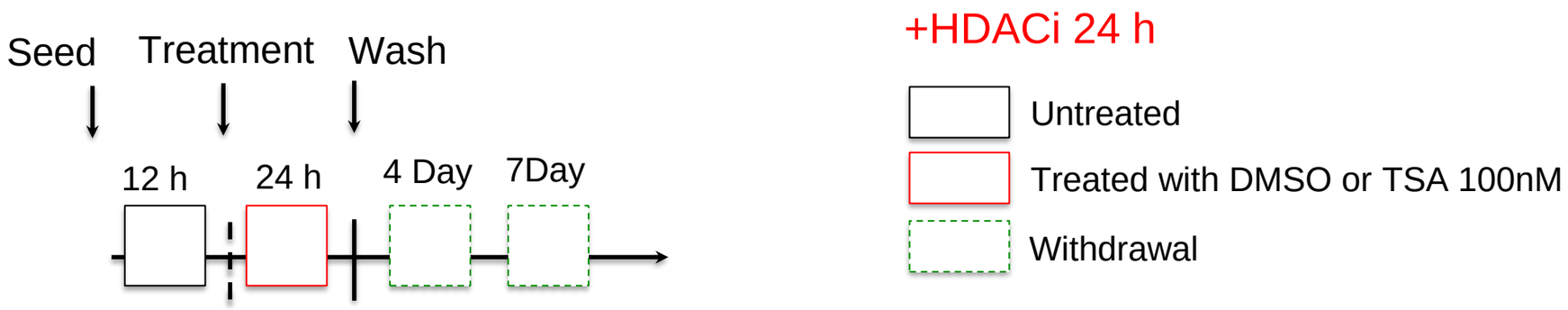


**B**

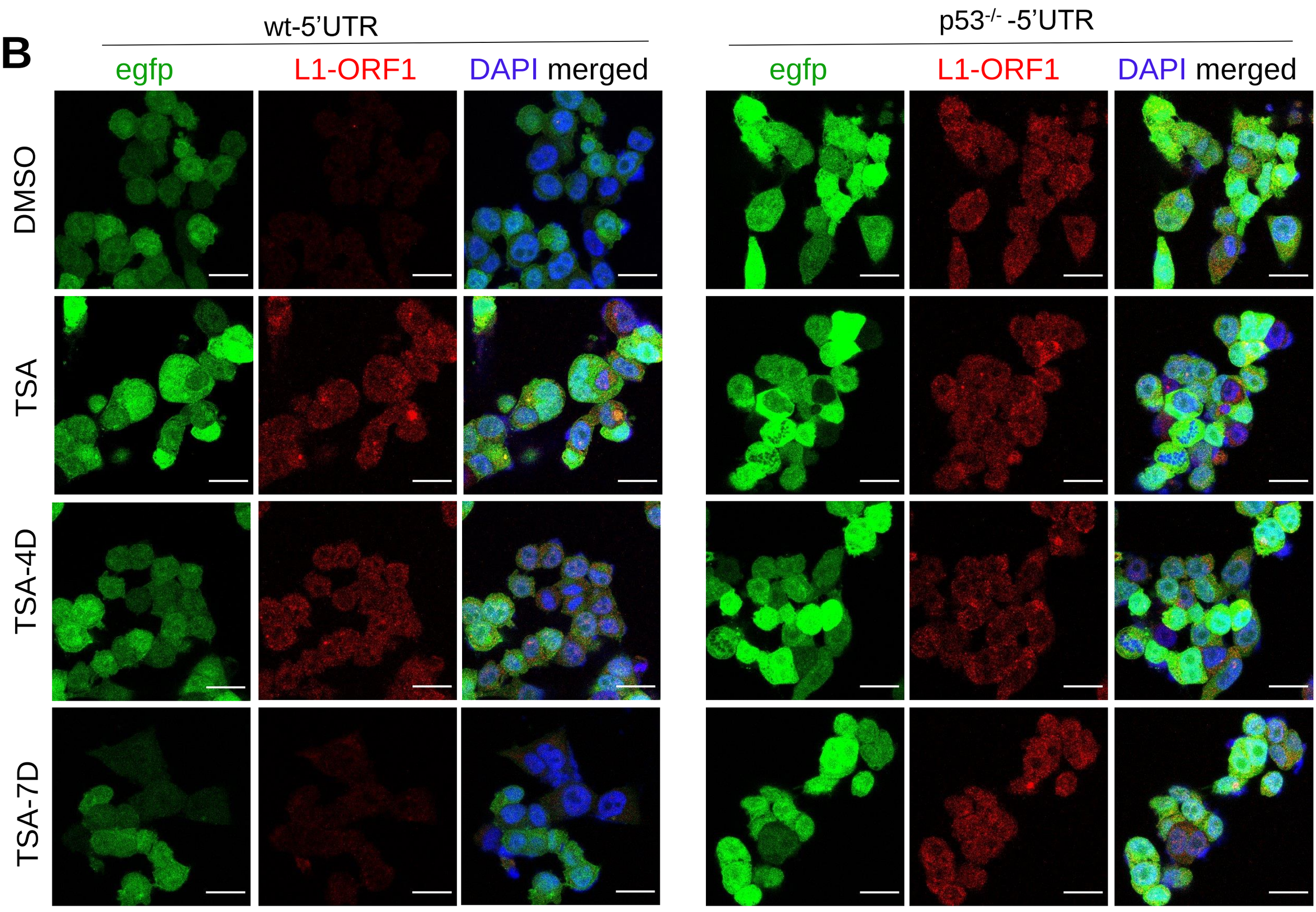


**C**

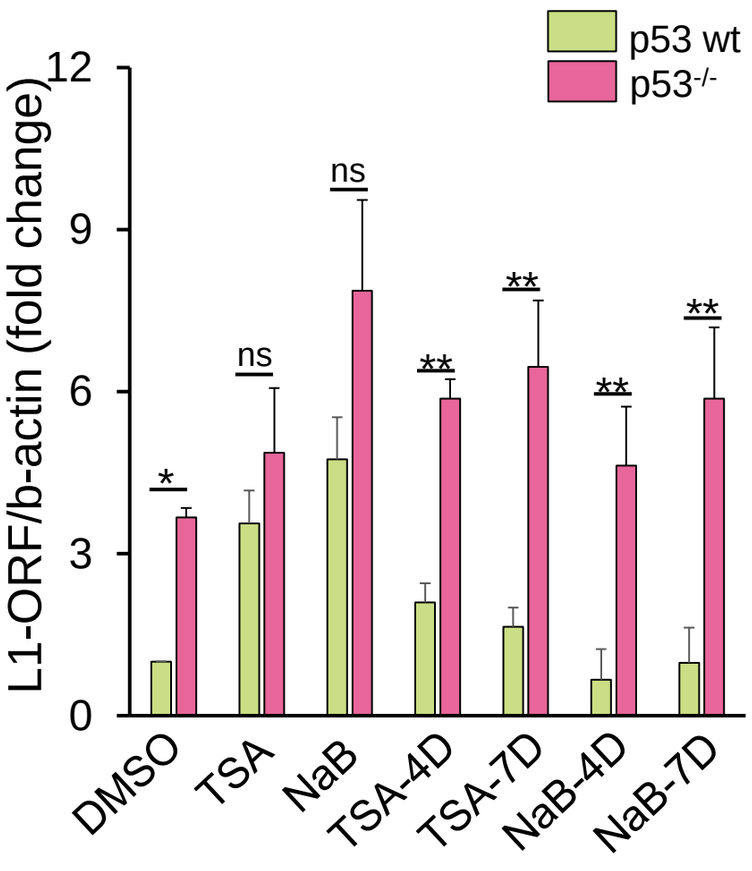


**D**

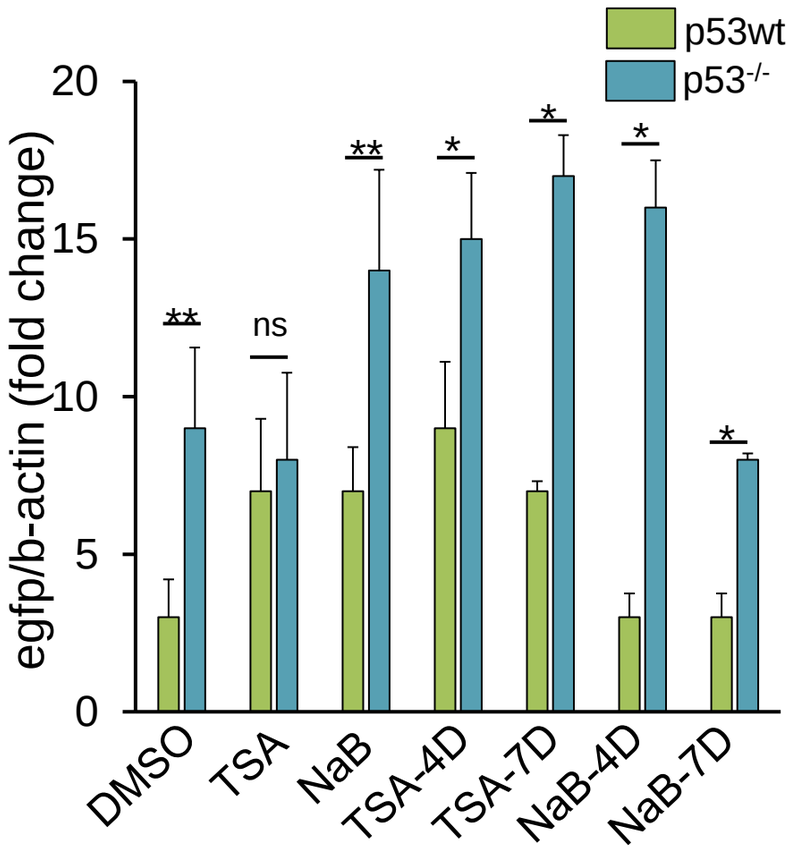


**E**

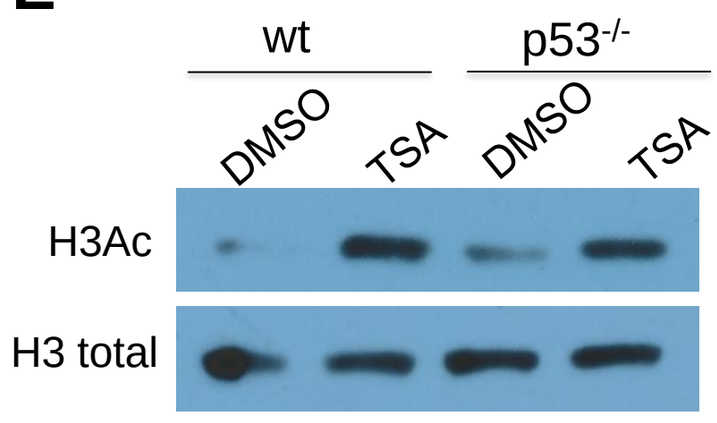


**F**

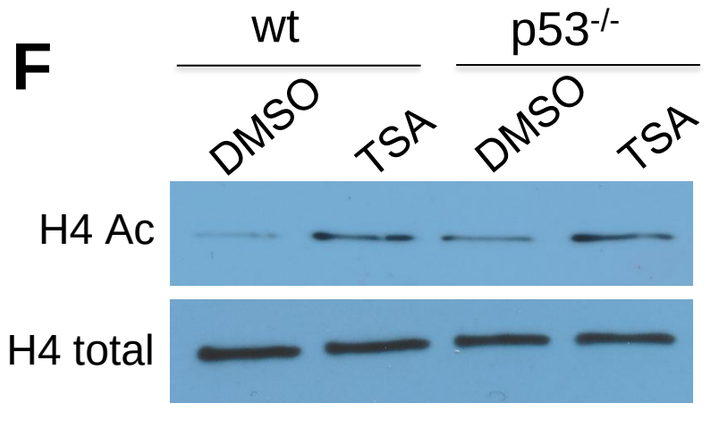

# Figure 5

## A

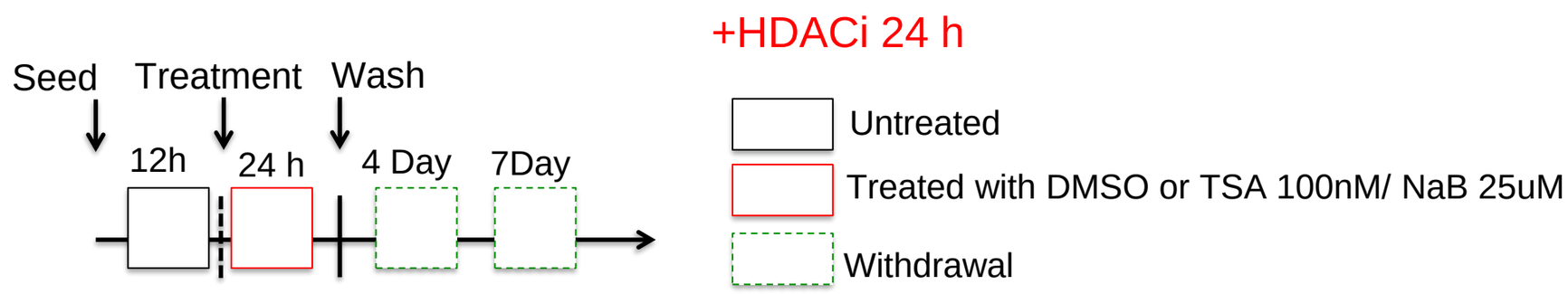


## B

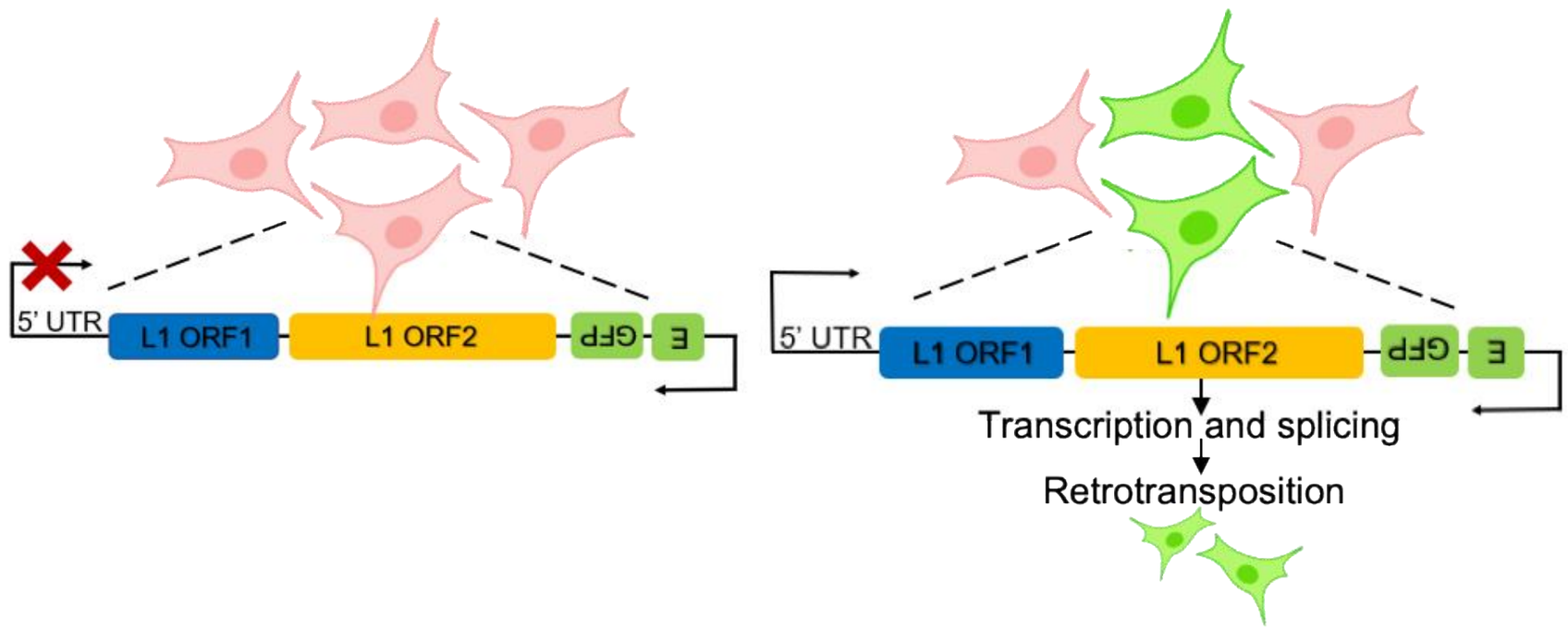


## C

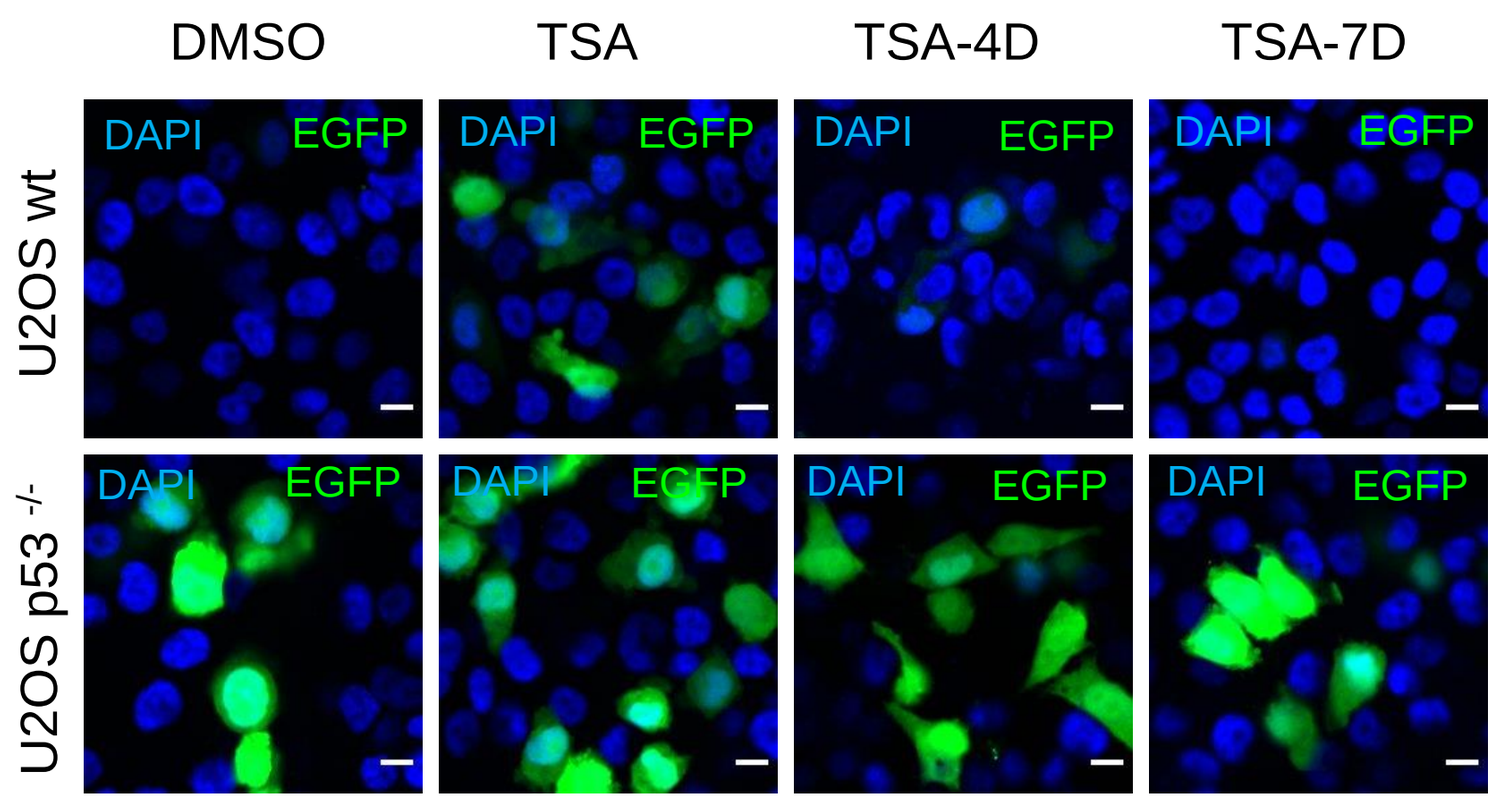


## C'

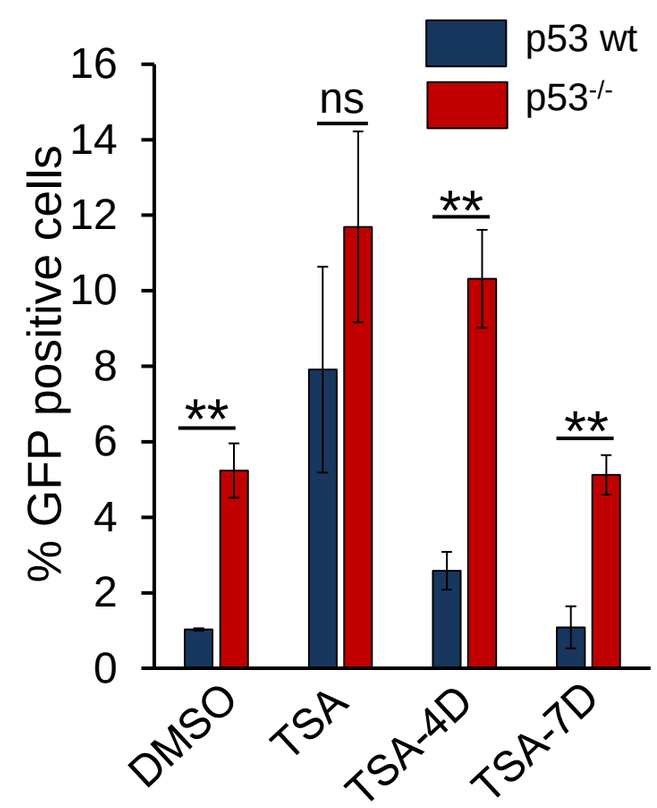


## D

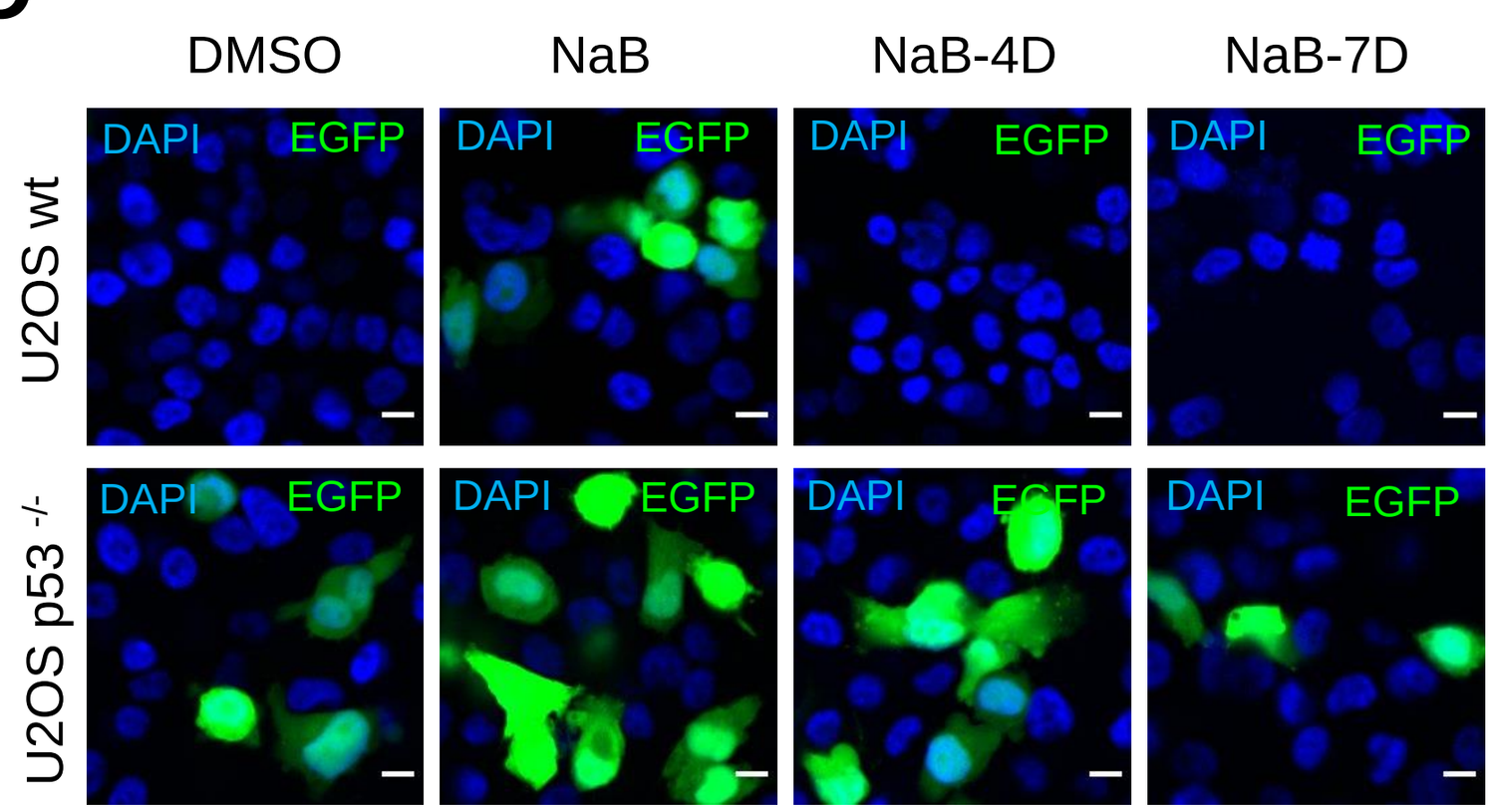


## D'

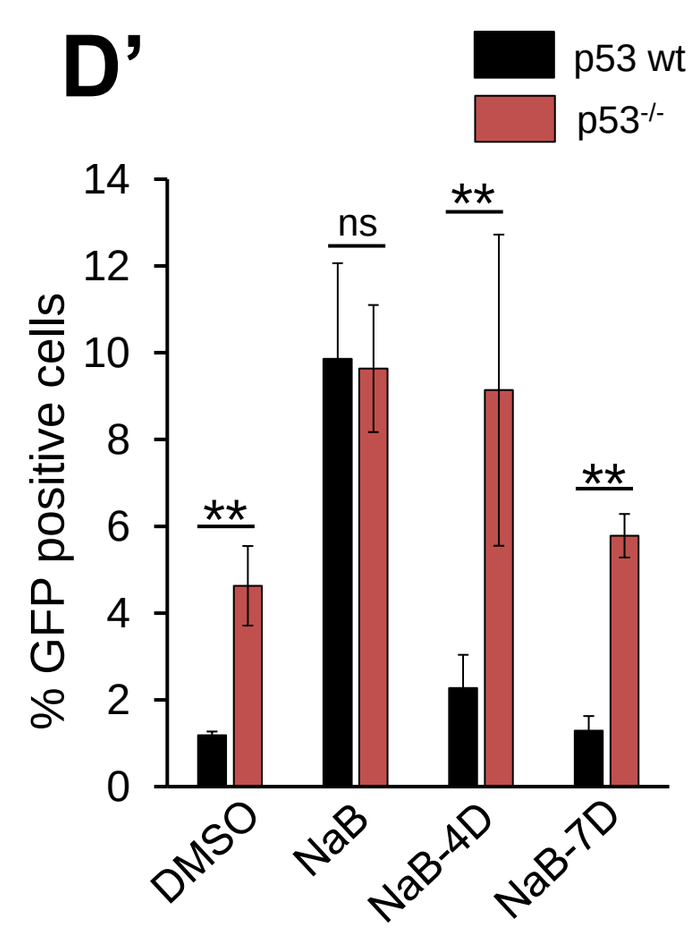

# Figure 6

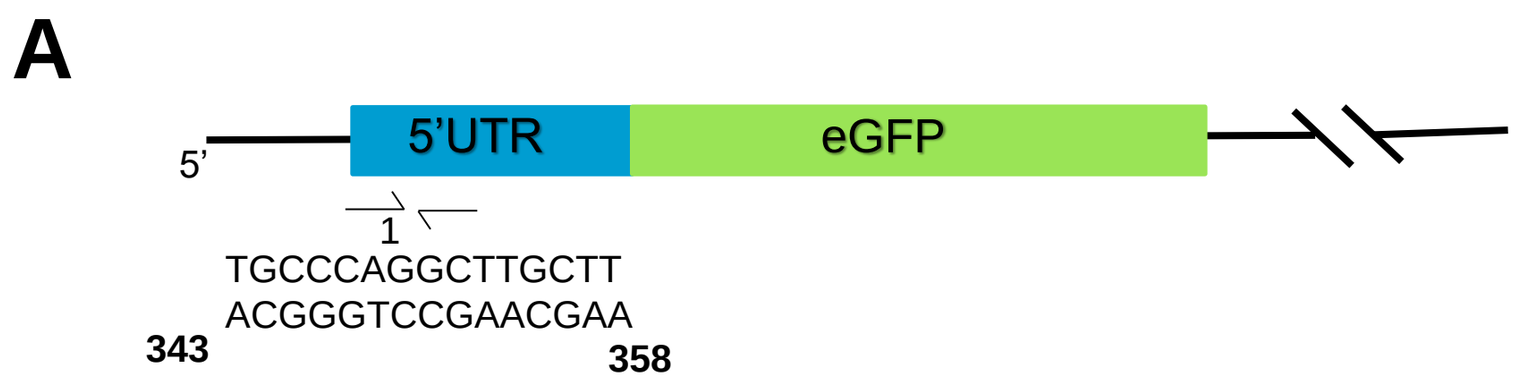
A
5'
5'UTR
eGFP
1
TGCCCAGGCTTGCTT
ACGGGTCCGAACGAA
343
358

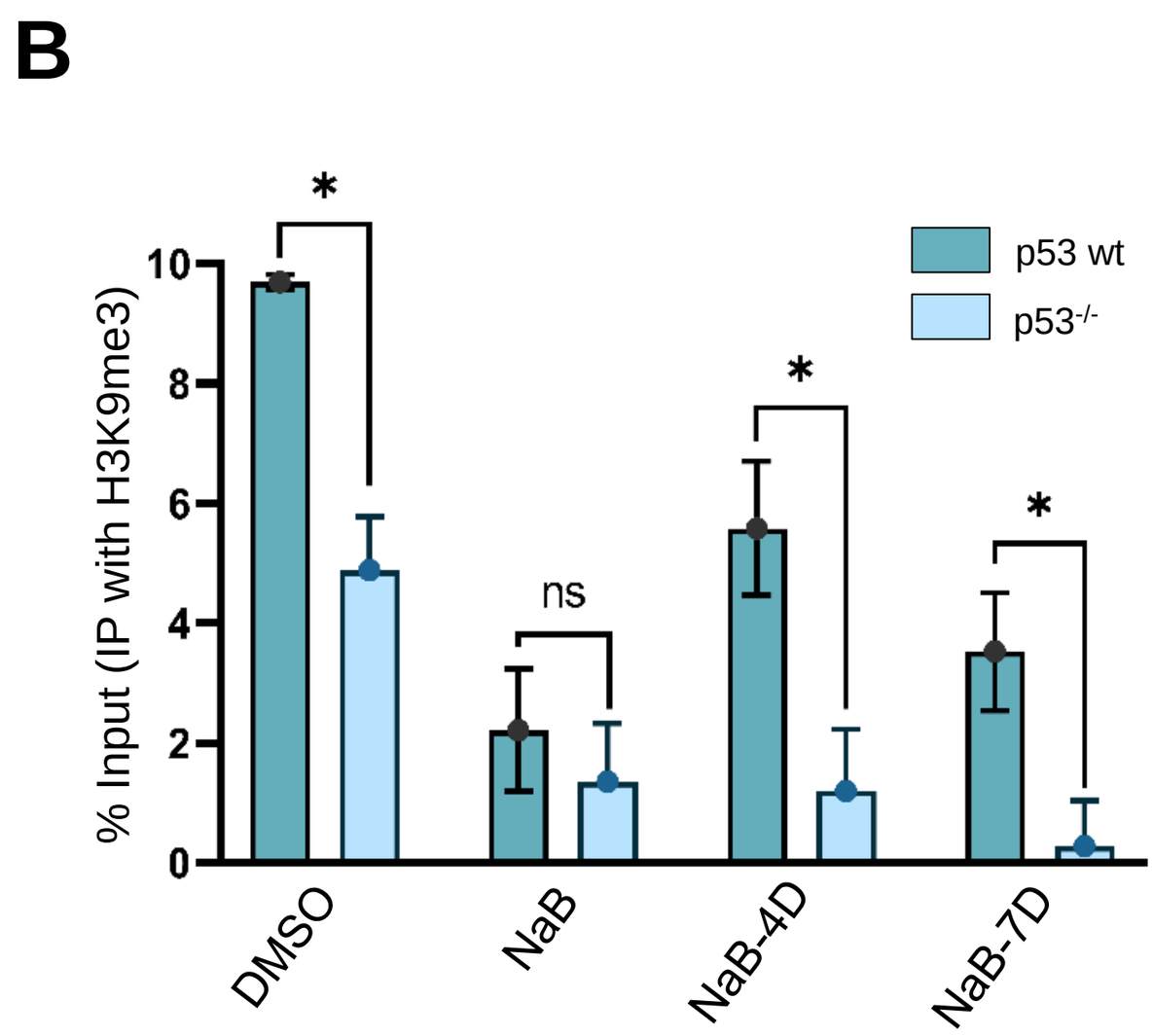
B
% Input (IP with H3K9me3)
p53 wt
p53-/-
*
ns
*
*
DMSO
NaB
NaB-4D
NaB-7D

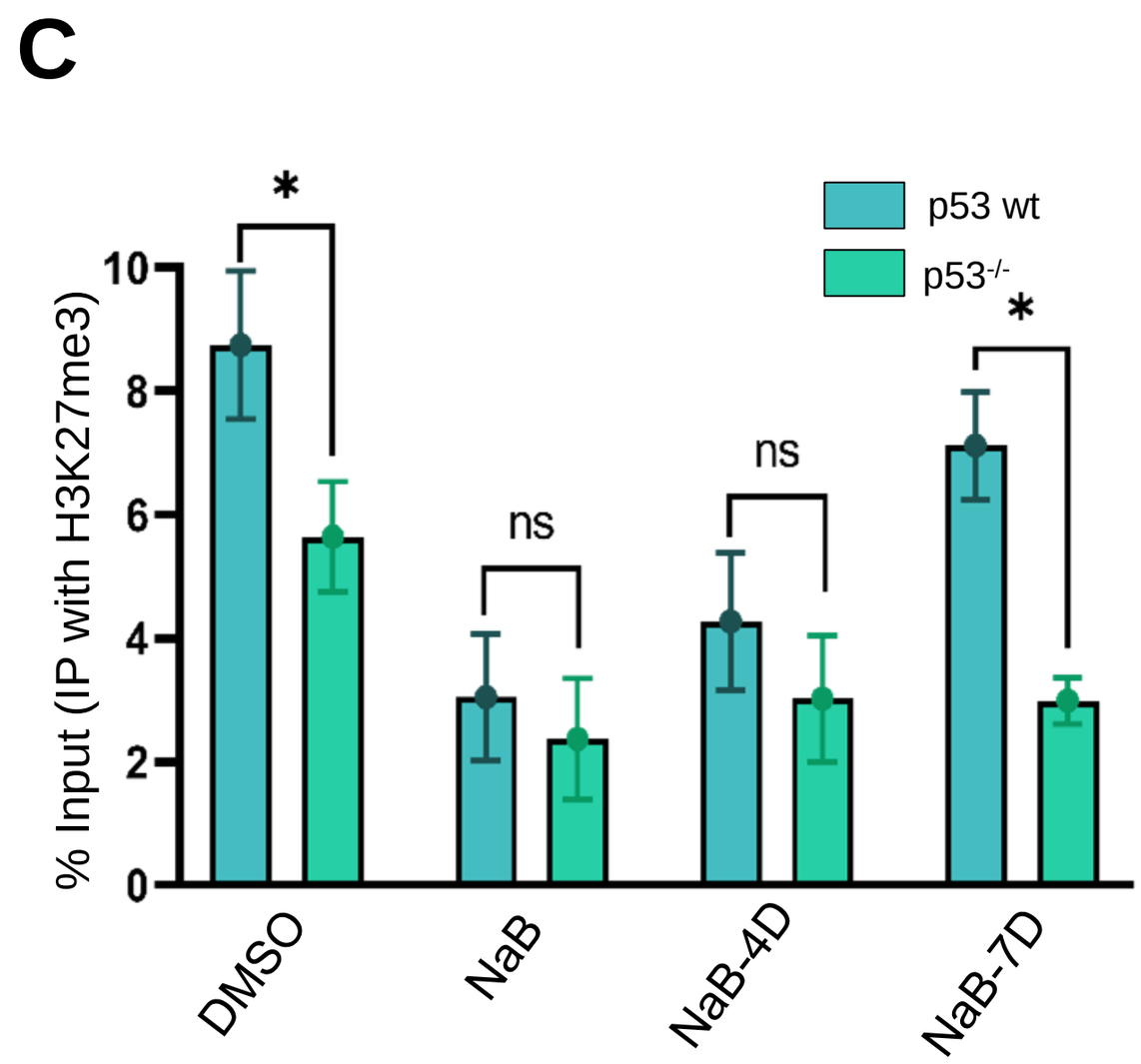
C
% Input (IP with H3K27me3)
p53 wt
p53-/-
*
ns
ns
*
DMSO
NaB
NaB-4D
NaB-7D

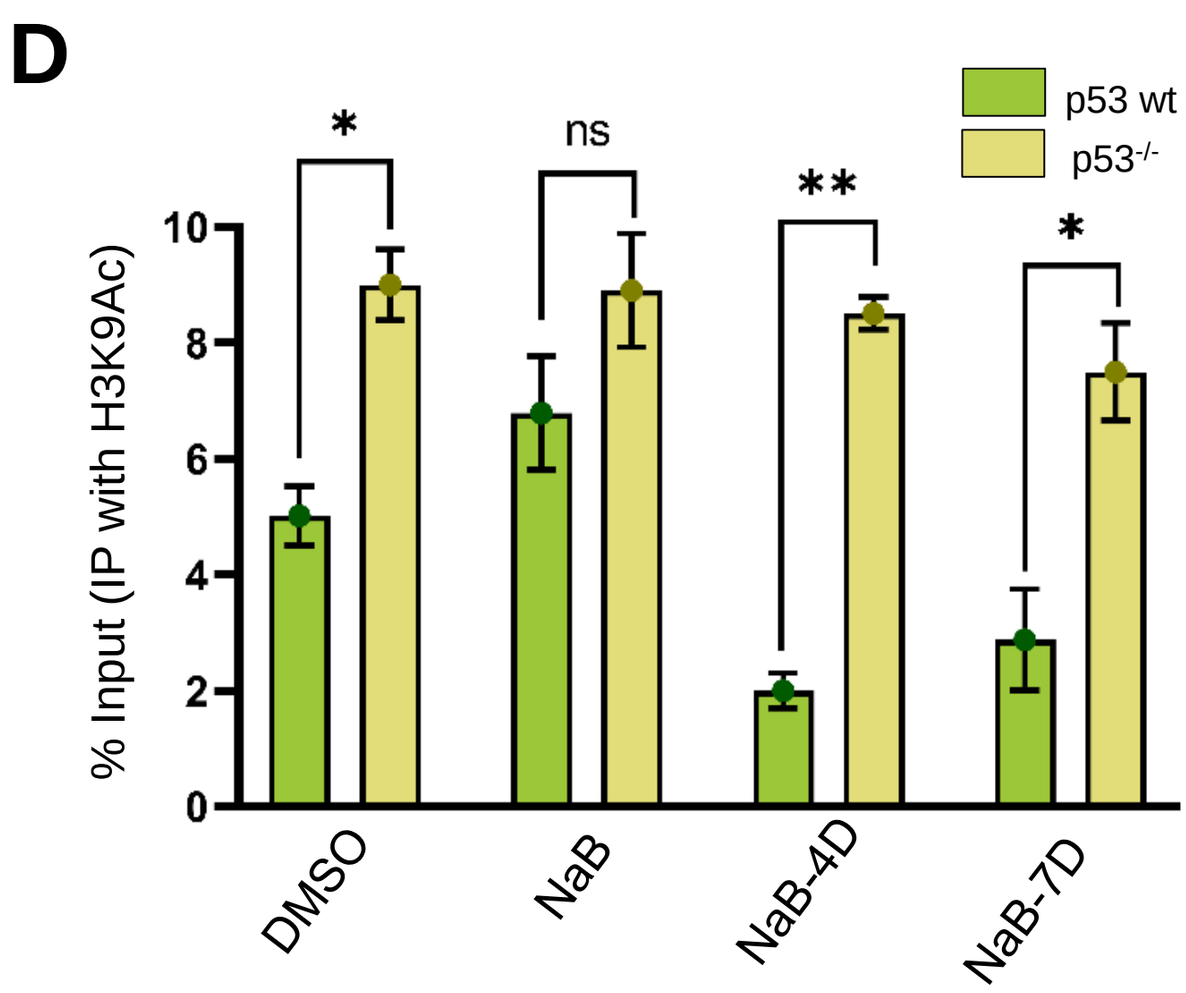
D
% Input (IP with H3K9Ac)
p53 wt
p53-/-
*
ns
**
*
DMSO
NaB
NaB-4D
NaB-7D

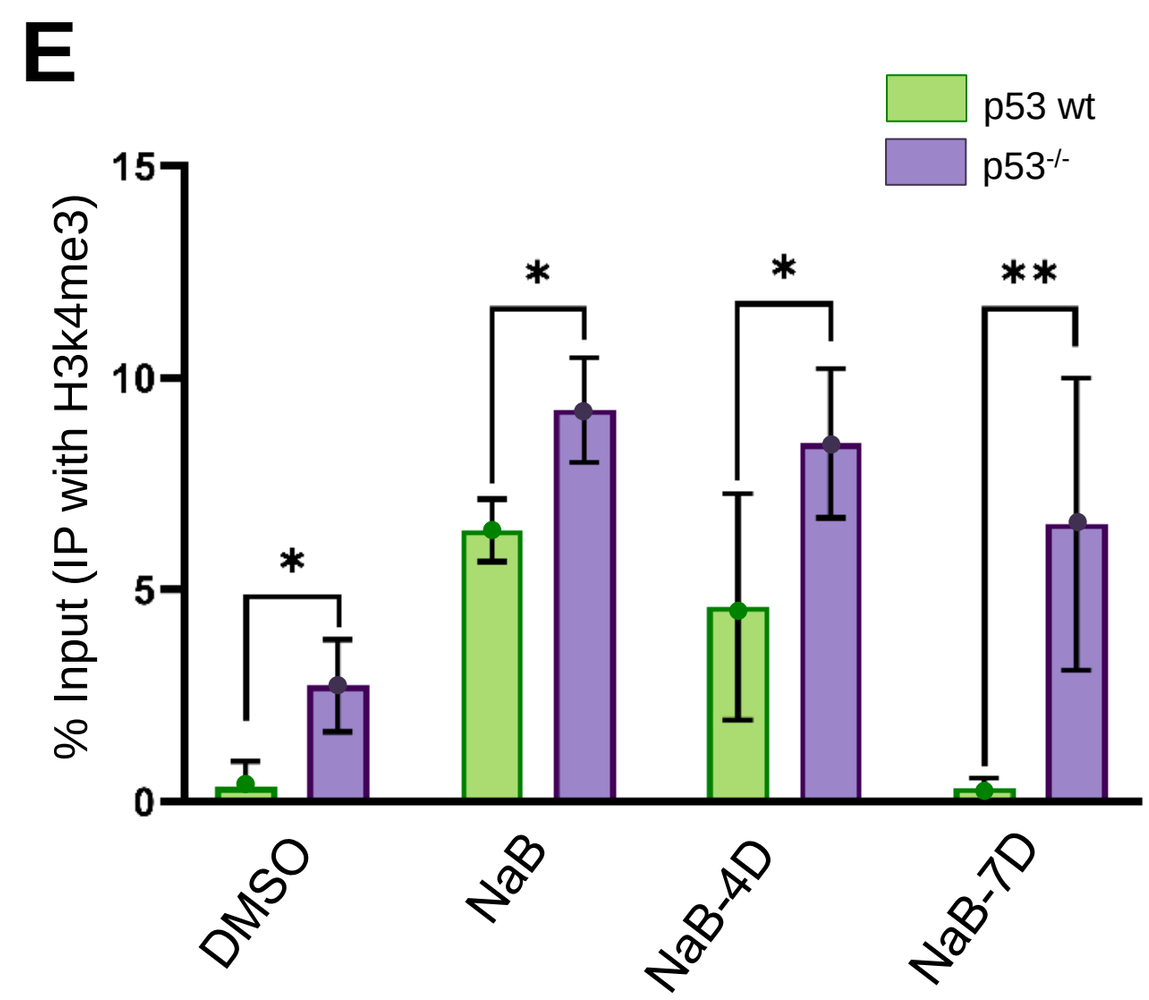
E
% Input (IP with H3k4me3)
p53 wt
p53-/-
*
*
*
**
DMSO
NaB
NaB-4D
NaB-7D

# Figure 7

## A

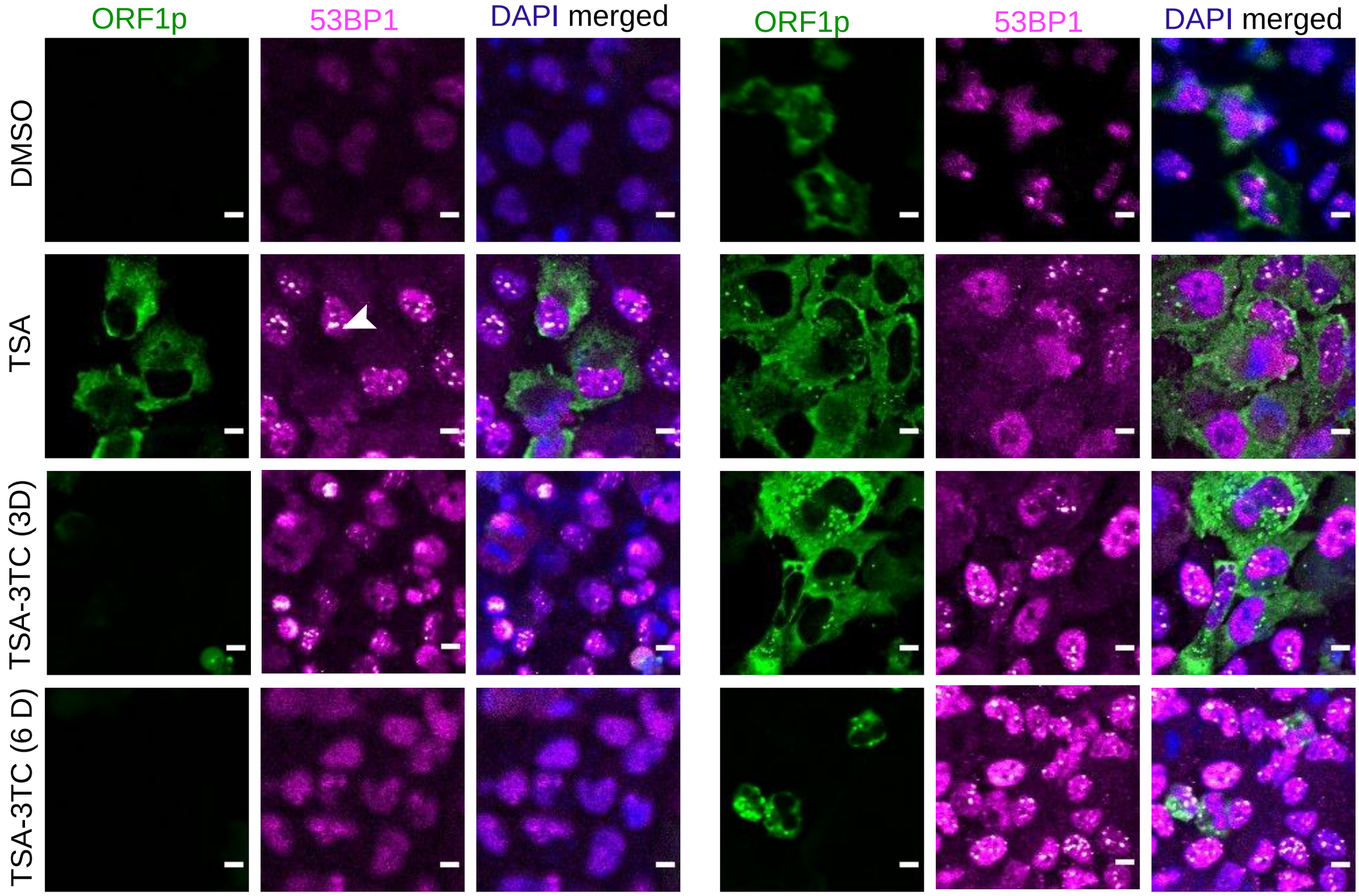
ORF1p
53BP1
DAPI merged
ORF1p
53BP1
DAPI merged
DMSO
TSA
TSA-3TC (3D)
TSA-3TC (6 D)

## A'

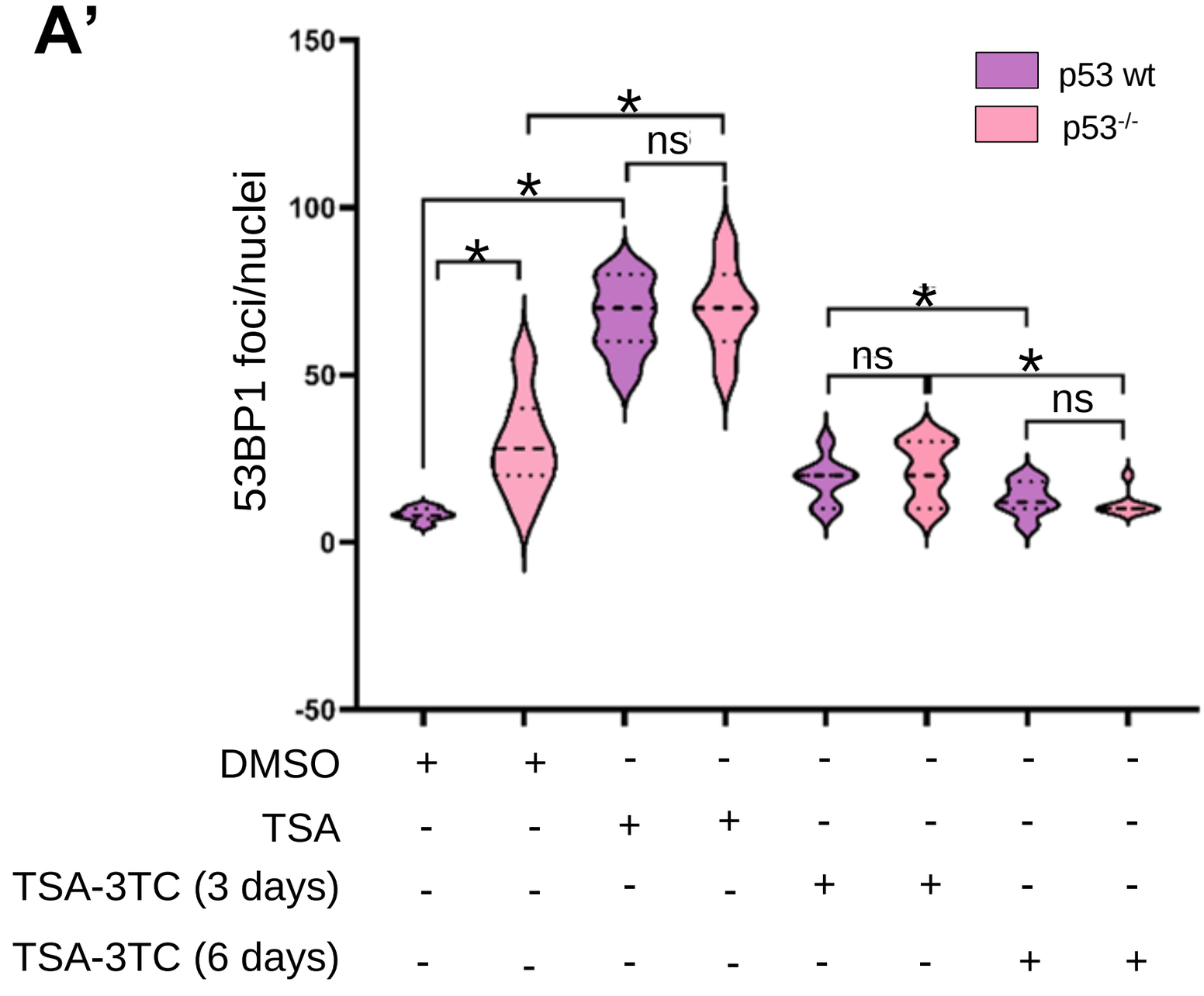
53BP1 foci/nuclei
150
100
50
0
-50
p53 wt
p53-/-
*
ns
*
*
*
ns
*
ns
DMSO + + - - - - - -
TSA - - + + - - - -
TSA-3TC (3 days) - - - - + + - -
TSA-3TC (6 days) - - - - - - + +